Fall 2016

Comparative Characterization Of Molybdenum Oxide Thin Films Grown On Various Substrates Using Temporally Different Pulsed Laser Deposition Techniques

Krishna Harsha Puppala

COMPARATIVE CHARACTERIZATION OF MOLYBDENUM OXIDE THIN FILMS GROWN ON VARIOUS SUBSTRATES USING TEMPORALLY DIFFERENT PULSED LASER DEPOSITION TECHNIQUES

A Masters Thesis

Presented to

The Graduate College of

Missouri State University

In Partial Fulfillment

Of the Requirements for the Degree

Master of Science, Materials Science

By

Krishna Harsha Puppala

December 2016

COMPARATIVE CHARACTERIZATION OF MOLYBDENUM OXIDE THIN FILMS GROWN ON VARIOUS SUBSTRATES USING TEMPORALLY DIFFERENT PULSED LASER DEPOSITION TECHNIQUES

Physics, Astronomy and Materials Science

Missouri State University, December 2016

Master of Science

Krishna Harsha Puppala

ABSTRACT

Pulsed Laser Deposition (PLD) technique, with its vast tunability in terms of thin film fabrication has been the center of this study. By changing the temporal component of the laser source used for deposition into the femtosecond (fs) regime, interesting structural, morphological changes can be achieved which may prove to be beneficial for photocatalytic applications. In particular, molybdenum oxide thin films, which are the less well-studied and potentially newer candidates for photocatalysis applications have been chosen for investigation. Hence, a detailed characterization study of molybdenum oxide thin films synthesized using femtosecond-based (f-PLD) and nanosecond-based (n-PLD) techniques, was carried out in terms of their structural, morphological, surface chemical/ electronic states and vibrational properties using X-ray diffraction, scanning electron microscopy, X-ray photoelectron spectroscopy and Raman spectroscopy. The f-PLD technique was found to produce more favorable molybdenum oxide thin films deposited on glass for surface-related applications, in terms of having a higher surface to volume ratio, than the n-PLD technique. A related simultaneous study of substrate-based effect on the thin films produced using n-PLD system, also revealed both variation among the morphological, structural, and electronic (in terms of Mo oxidation state) properties depending upon the nature of the substrate used to synthesize the molybdenum oxide thin films. Special cases of thin films on epitaxial substrates (Si, sapphire) have been characterized to determine the parameters necessary for fabricating highly-textured thin films with large surface-area to volume ratio, which is key to efficient photo-catalysts.

KEYWORDS: Thin films, Raman, SEM, XPS, Pulsed Laser Deposition

This abstract is approved as to form and content

_____

Robert A Mayanovic, PhD
Chairperson, Advisory Committee
Missouri State University

COMPARATIVE CHARACTERIZATION OF MOLYBDENUM OXIDE THIN FILMS GROWN ON VARIOUS SUBSTRATES USING TEMPORALLY DIFFERENT PULSED LASER DEPOSITION TECHNIQUES

By

Krishna Harsha Puppala

A Masters Thesis
Submitted to the Graduate College
Of Missouri State University
In Partial Fulfillment of the Requirements
For the Degree of Master of Science, Materials Science

December 2016

Approved:

_____
Robert A Mayanovic, PhD

_____
Mahua Biswas, PhD

_____
Fei Wang, PhD

_____
Julie Masterson, PhD: Dean, Graduate College

ACKNOWLEDGEMENTS

I will always be thankful and indebted to my advisor, Dr. Robert Mayanovic for his unending support and patience towards my thesis completion. His enthusiasm to mentoring and teaching others has inspired me all along the way. It has been his continuous belief in my success that had led to my successful completion of this thesis. I shall always be indebted to Dr. Mahua Biswas and Dr. Fei Wang for serving on my thesis committee and guiding me at all crucial stages of this work. I shall always be grateful to Dr. Kartik Ghosh, Dr. David Cornelison and Dr. Ridwan Sakidja for helping me at various stages of this thesis.

My special thanks to fellow colleagues, Mr. Delower Hossain, Mr. Tamzid Ibn Minhaj, Mr. Anthony Pelton and Mr. Abdullah Mamun for helping me professionally with this research work. I must specially thank Jake Connor, of US Photonics for collaborating with our research group under Dr. Robert Mayanovic and showing immense interest in this work. I would like to thank Laura Rios, the department's administrative assistant, whose constant help throughout my graduate study is worth mentioning. Also, I would like to acknowledge Rishi Patel, for providing help with the XPS data collection.

It was the never ending faith in my success among my parents, friends and family that made this work possible. Finally, I would like to thank the Graduate College for providing partial support towards this research work.

I dedicate this thesis to Madhavi (Mother) and Mohan Rao (Father).

TABLE OF CONTENTS

LIST OF TABLES

LIST OF FIGURES

CHAPTER 1: INTRODUCTION

The pulsed laser deposition (PLD) technique is a highly versatile method for thin film deposition performed by ablating a target with a high energy pulsed laser in a controlled vacuum chamber. In particular, it is unique in that the technique allows for the deposition of a wide range of thin films (e.g., metal oxides, nitrides, germinates, arsenides, etc.) not accessible to other deposition techniques. While the target material of interest is being ablated by the pulsed UV-laser, a plasma plume is created consisting of high velocity energetic species. These in turn travel towards a nearby substrate, which may or may not be heated, to subsequently condense on its surface forming a stoichiometric thin film [1]. The main advantage of the PLD technique is that it can create materials with complex stoichiometry while keeping the particle size distribution to a small range, while keeping the impurities to relatively low level [2]. The high-power pulsed UV-lasers in a vacuum chamber environment enable the creation of a variety of stoichiometric oxide films, especially when used in combination with a reactive background gas atmosphere. Although the reactive atmosphere does not affect the laser beam path and its interaction with target materials, it does have a bearing on the plasma plume creation and its kinetics [3]. Over the years, the PLD technique has been developed into a reliable methodology for the fabrication of high purity, functional thin films necessary for device manufacturing. The high purity of the thin films created in this way is an outstanding feature of the PLD technique; nevertheless, it should be noted that this is highly dependent upon the level of vacuum in the chamber and care taken to ensure high purity of substrate, ambient gas and target used in PLD. The disadvantage of

this fabrication process while using the nanosecond –based laser is the formation of bulk particulates which travel within the created plume toward the colder substrate surface during deposition. These bulk-type deposits (often called “splashing”) are due to the extreme thermal shock imposed upon the target surface by the impinging laser pulses. More recently, some developments have been made to counter these relatively slow-moving particulates from the plasma, such as, a velocity-based mechanical particle filter [3]. However, the thrust of PLD technique development has concentrated on the removal of these particulates during initial creation at the source, i.e., at the target. Irrespective of the type of the deposition technique of the thin films, the adhesion of the thin films to the substrate also plays a key role in its usefulness for practical applications. The main reasons behind adhesion of thin films could be primarily due to atomic bonds created by the interaction of the two surfaces, or mechanical locking and friction due to surface texture and an inter-diffusion transition layer formed at the interface [4]. Hence, there is a dual control nature embedded in the PLD synthesis of thin films: one being the ablation mechanism during the deposition process, and the other being the interface control of the substrate and thin film, during and after deposition process. These two primary control variables should be well understood and monitored before the production of a thin film applicable to any type of real-life purpose.

Whereas the majority of current research is focused on the synthesis of nanostructured thin films by PLD using nanosecond (ns)-based lasers (pulse duration~10^{-9} seconds), the use of femtosecond (fs) –based laser (pulse duration<10^{-15} seconds) has been made sparingly. A typical nanosecond excimer laser-based PLD chamber is represented in the schematic diagram provided in F 1.1 [5]. While many other studies

were made using variable stoichiometric targets to create complex multicomponent oxides and compounds, considerably less is known on the usage of picosecond- & femtosecond-based laser (pulse duration~10^{-12} - 10^{-15} seconds order magnitude). As such, the use of femtosecond-based laser for PLD could be a potential game changer for production of thin films for photocatalytic applications. This research in part attempts to fill upon the gap produced in between the comprehension of both these techniques and their applicability to create high surface-area to volume ratio structures.

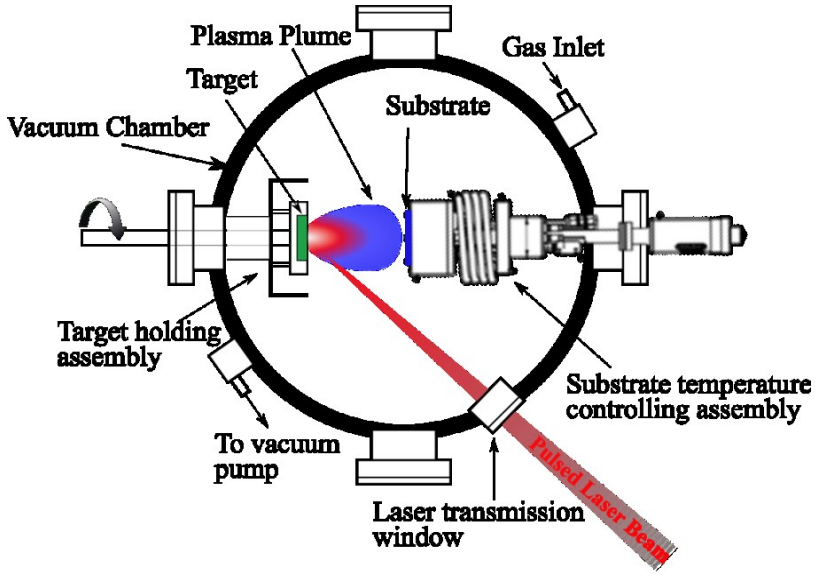

Figure 1.1. A schematic of the excimer laser-based PLD chamber setup used for the n-PLD based thin films [5].

Femtosecond Pulsed Laser Deposition

The ultra-short laser pulses of the femtosecond-pulsed lasers provide a unique advantage of energy minimization at the surface of the target material, thereby avoiding the thermal energy dissipation into the bulk that is inherent in the use of nanosecond excimer based laser PLD [6]. The femtosecond ranged pulsed laser-matter interaction also maintains the surface density of a given solid target constant throughout the laser

ablation. This enables a cleaner ablation process that avoids creation of molten droplets and enhances the synthesis of stoichiometrically pure thin films [1]. In addition, the ultrashort pulsed ablation method inherent in the use of the femtosecond-pulsed laser tends to reduce the formation of the splashes on the substrates, which is a major issue in the conventional excimer laser processes, especially in the deposition of metal oxide systems. This is because the short-pulse interactions limit the relaxation dynamics and the seeking of thermal equilibrium by the target species (i.e. molecular, atomic, etc.), which is in contrast to the interactions produced by the longer nanosecond pulses. Hence, the result is an achievement of highest possible laser intensities ($>10^{13}$ W/cm^2), when compared to any known laser ablation method used till date [6]. The femtosecond lasers are relatively newer types of temporally adjusted photon sources which have been predominantly used for industrial micro-machining applications demanding high precision. Use of these femtosecond high-intensity lasers provides an ablation process whereby the multiphoton ionization and avalanche ionization are the determining absorption mechanisms within the surface of the target material. These mechanisms provide a means by which the lasers' energy is absorbed to a maximum extent at the target, which would not be possible using a conventional low intensity nanosecond-based laser.

Molybdenum Oxide Thin Films as Candidate Materials

The orthorhombic phase of molybdenum trioxide (α-MoO_3), has the basis of MoO_6 octahedral unit repeated in an orthorhombic lattice. These octahedral building blocks are corner-shared so as to form chains of edge-shared layers (F 1.2 (a)). These

layers are arranged on top of one another in a zig-zag manner where the layers are held together by Van der Waals forces [7]. The crystal structure of α-MoO_3 consists of a layered structure of two octahedral MoO_6 layers, joined by double covalent forces in the a and c axes. The layers are attracted by Van der Waal's forces along the b axes [8]. The anisotropic growth of these crystallites is a consequence of distorted MoO_6 octahedral units (unequal Mo-O distances along the O-Mo-O bond direction) which form the lattice of MoO_3 [9]. It is the layering inherent in the alpha phase that makes it highly suitable for many practical applications, especially in catalysis, battery storage technology, smart windows, and other electrochromic-based technologies. The orthorhombic structure is thermodynamically most stable polymorph of MoO_3, even though it has numerous oxidation states ranging from +2 to +6 with each having its own crystal system. Sub-stoichiometric thin film oxides have been studied recently for specialized applications. In its native form, MoO_3 is a wide band gap n-type semiconductor transition metal oxide. The semiconductor band gap is generally found to be approximately 2.6 eV, but also varies from 2.8 – 3.2 eV. The oxide is also known to have the metastable-monoclinic (β-MoO_3) and hexagonal (h-MoO_3) phases. While the monoclinic β-MoO_3 has a resemblance to the perovskite-like structure (ReO_3-type) with a continuous network of corner-shared MoO_6 octahedral units (F 1.2 (b)), the hexagonal phase is also a metastable polymorph with a zig-zag arrangement of distorted MoO_6 octahedra in a cis-position [10]. Molybdenum dioxide (MoO_2) forms when the metal is in the Mo^{4+} oxidation state. The MoO_2 crystal structure consists of a distorted rutile-type tetragonal crystalline arrangement [11]. It has been shown that the phase transition of β to α- MoO_3 occurs at above 350 °C.

The recent past has seen the growth of MoO_3 films for gas sensors, lithium ion batteries, electrochromic device applications and many more. The principal techniques used for synthesis of metal oxide films have been (RF and DC) sputtering, chemical vapor deposition (CVD), and PLD techniques. PLD has been used for growth of molybdenum oxide thin films by Kuhaili et al [12] & Pardo et al [13] and others.

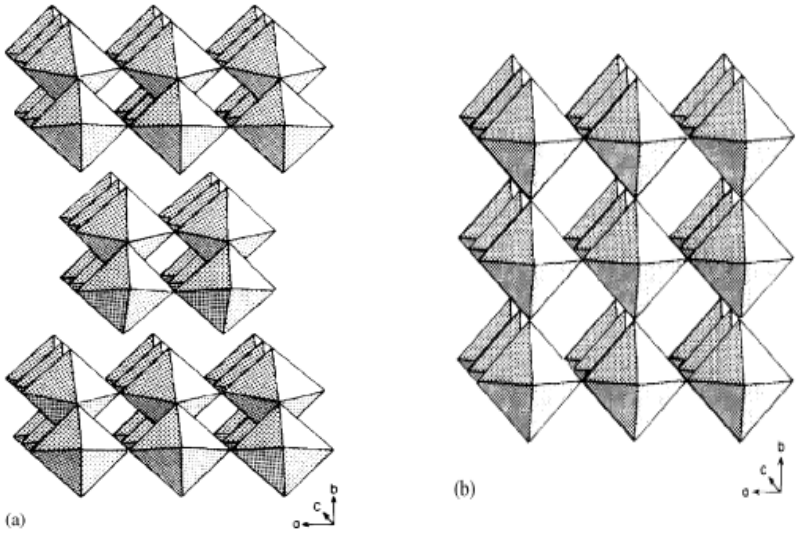

Figure 1.2. The crystal structures of (a) orthorhombic α- MoO_3 (b) ReO_3 –type monoclinic β- MoO_3 [7].

Annealing Effects and Substrate Based Studies

While it has been largely accepted that annealing at temperatures above 400 °C in requisite oxygen-bearing atmospheres leads to ideal stoichiometry attainment of O: Mo = 3:1, there has been debate as to what effect the temperature choice has on the crystallization of these thermodynamically stable hexavalent phases. Annealing in oxidizing temperature above 400 °C has been shown to accommodate the improvement of the atomic ordering within the films [14]. However, another important aspect in

temperature selection is whether the desired short and long range atomic ordering is achieved at the chosen annealing temperature.

In Chapter 2 of this thesis, a comparative study of femtosecond- and nanosecond-based PLD of molybdenum oxide thin film deposited on glass substrates is presented. This work has been published in MRS Advances [15]. In Chapter 3 of this thesis, I present a comparative study of molybdenum oxide thin films synthesized using nanosecond-based PLD and deposited on glass, silicon and sapphire substrates. This work is in preparation for submission to the journal Thin Solid Films.

CHAPTER 2: A COMPARATIVE CHARACTERIZATION STUDY OF MOLYBDENUM OXIDE THIN FILMS GROWN USING FEMTOSECOND AND NANOSECOND PULSED LASER DEPOSITION

Abstract

Group 6 transition metal oxide thin films are in large demand for photocatalysis, heterogeneous catalysis, fuel cell, battery and electronic applications. Pulsed laser deposition offers an inexpensive method for the preparation of nanostructured thin films that may be suitable for heterogeneous catalysis. I have synthesized molybdenum oxide thin films using two types of pulsed laser deposition (PLD). The first method utilizes femtosecond laser-based PLD (f-PLD) while the second method uses an excimer (nanosecond) laser-based PLD (n-PLD). The PLD films have been deposited using f-PLD and, separately, n-PLD on glass and silicon substrates and subsequently annealed to 450 °C for up to 20 hours in air using a Linkam stage. SEM, XRD and Raman spectroscopic characterization shows that the f-PLD films are substantially more textured and partially crystalline prior to annealing whereas the n-PLD-grown thin films are much smoother and predominantly amorphous. A 3-dimensional nano-crystalline structure is evident in the post-annealed f-PLD synthesized thin films, which is desirable for catalytic applications. XPS elemental analysis shows that the stoichiometry of the f-PLD and n-PLD thin films is consistent with the presence of MoO_2 and MoO_3. My results are discussed in terms of thin film growth models suitable for f-PLD vs n-PLD.

Introduction

The transition metal oxide thin films have a significant role to play in major energy applications like photocatalysis, heterogeneous catalysis, electrochromic and photochromic devices etc. [1]. Molybdenum trioxide (MoO_3) is highly useful as a selective catalyst for hydrocarbon oxidation [2, 3]. Crystalline molybdenum trioxide occurs in two major crystal phases, namely orthorhombic α-MoO_3 and monoclinic β-MoO_3. The α-MoO_3 phase is thermodynamically stable and the β-MoO_3 is metastable [4]. While the amorphous molybdenum oxide thin films have a perovskite-like structure consisting of corner-shared MoO_6 octahedra, they have been shown to exhibit more photochromic response than their crystalline counterparts [1]. The band gap of molybdenum trioxide can be modified by various means, including introduction of dopants and by ionic (e.g., alkali ions) intercalation. The synthesis of these thin films falls into three major categories: vapor, liquid and solid phase deposition techniques. The common element of these techniques is the aim to increase the planar area of the preferred growth of the layered material, have control over the film thickness, and to produce films having good crystallinity [4]. There is currently considerable interest in the relatively low-cost synthesis of thin films having novel nanostructured properties for projected future applications in energy harvesting and industry. Femtosecond lasers may find suitability for use in thin film deposition as these have higher intensities and shorter pulse durations than nanosecond lasers currently used in pulsed laser deposition (PLD). Femtosecond laser PLD (f-PLD) has been used in the past by a handful of workers for deposition of thin films where it has shown promise for synthesis of materials having novel properties [5-7]. Additionally, f-PLD films may eliminate the issue of macroscopic

droplet formation, which is considered to be the result of thermal effects during the laser-matter interaction [8]. Herein, I discuss some of the results from the growth of molybdenum oxide thin films using f-PLD and compare those to the characteristics of molybdenum oxide thin films prepared using nanosecond laser PLD (n-PLD).

Experimental

The MoO_3 targets used for pulsed laser deposition were prepared from pure (>99%) MoO_3 powder (Sigma-Aldrich). The powders were ground very finely using mortar and pestle and compressed into pellets using a 10 Metric-ton hydraulic press. Polyvinyl alcohol (PVA) was used as the binding agent during powder mixing. The pressed MoO_3 targets were sintered in the 650-690 °C temperature range for at least 12 hours. The deposition of the molybdenum oxide thin films was made in separate chambers set up for f-PLD and n-PLD. The f-PLD thin films were prepared using a Ti: sapphire femtosecond laser of wavelength 800 nm at US Photonics whereas the n-PLD films were synthesized using a 248 nm UV excimer laser. The films were deposited on clean microscopic glass slides and single crystal Si substrates. The n-PLD was made under Oxygen atmosphere, with oxygen introduced into the chamber at a rate of ~1.5 ccm. The thin films were annealed at 450 °C for varying annealing times. Structural and morphological study was done using FESEM (FEI-Quanta 200) instrument operating at 20 kV. The Scanning electron microscopy (SEM) imaging was made by mounting the thin film samples on the Cu and C tapes. Preliminary chemical analysis was done with the help of SEM-EDX by using a field emission gun (Oxford Instruments). X-ray diffraction (XRD) measurements were made using a Bruker D8 Discover instrument

operating at 40 kV and 40 mA. The XRD instrument with a characteristic X-ray source of Cu tube (Cu Kα, λ= 1.54184 Å) was used. The Raman spectroscopy was made on the samples using a Horiba LabRAM HR 600 with a green laser (532 nm). The Raman instrument was used with the employment of neutral density filters (D0.6, D1) in LabSpec software in order to reduce the incident laser intensity and eliminate laser damage to thin films. The optical system used on the LabRAM HR 600 were an Olympus confocal microscope (40X objective) with a 600 gratings/mm configuration. X-ray photoelectron spectroscopy (XPS) analysis was performed using Thermo Scientific Alpha 110 hemispherical analyzer with pass energy of 25 eV. Al K-α X-ray source was used for XPS analysis, which has a characteristic energy of 1486.6 eV. XPS data analysis of survey spectrums and high-resolution spectrum peak fitting was made using CasaXPS 2.3.16 software package with C 1s peak taken as a calibration reference for Binding Energy (284.8 eV).

Results and Discussion

In Figure 2.1, I show the SEM images of n-PLD and f-PLD thin films. The SEM images show that both prior- and post-annealing, the f-PLD films possess more nanostructured texture and higher relief morphology whereas the n-PLD films are predominantly amorphous and smooth. Although generally smooth, the pre-annealed n-PLD thin film does show some fine textured nano- to micron-sized particulates on its surface. This variation in morphology of the pre-annealed films may be due to the differences in the energetics of the plasma interacting with the substrate in the f-PLD vs n-PLD process. I note the stacked growth of the microcrystals after annealing of the n-

PLD thin film (Figure 2.1d). This suggests a preferred orientation (confirmed from XRD analysis as shown below) of most likely the orthorhombic α-MoO_3 but perhaps also the MoO_2 phase. Interestingly, the f-PLD thin film has a higher aspect ratio (and surface-to-volume ratio) after annealing than the n-PLD thin film. This is more desirable for many applications, such as in heterogeneous catalysis, where high surface-to-volume ratio is desirable.

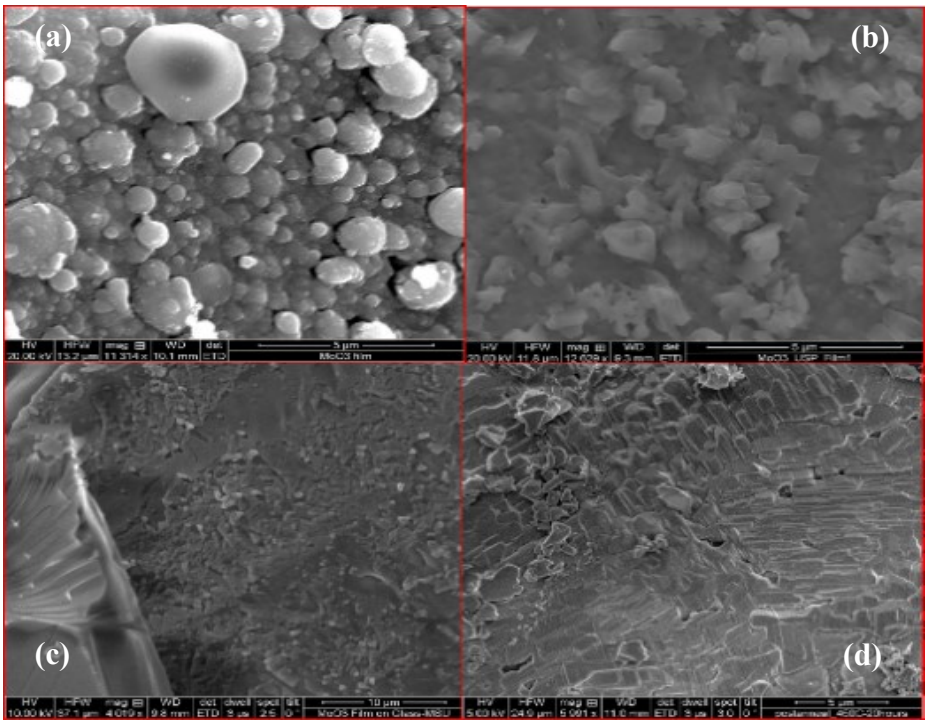

Figure 2.1. SEM micrographs (clockwise) showing the differences in the morphology of thin films prepared using f-PLD (a & b) and n-PLD (c & d). NOTE **:** The images at left show films prior to annealing (as-deposited) and those at right show films after annealing at 450°C.

The XRD patterns of the freshly prepared thin films show predominantly amorphous character with the f-PLD thin film showing some crystalline aspect as shown by the small peaks overlying the broad amorphous features (Figure 2.2). The XRD

patterns shown in Figure 2.2 (right panel) indicate presence of both the MoO_3 and MoO_2 in both the n-PLD and f-PLD post-annealed thin films. The XRD pattern for the n-PLD post-annealed film (Figure 2.2 right panel) clearly shows majority preferential orientation of the orthorhombic α-MoO_3 phase component with the preferred orientation along the (0k0) planes, where k=2, 4, 6.

The XPS high-resolution spectra of post-annealed f-PLD and n-PLD thin films are shown in Figure 2.3. I have used a Gaussian-Lorentzian product GL (30) function for fitting of the relatively symmetric line shapes in the high-resolution spectra shown in Figure 2.3. Table 2.1 shows the results from fitting of the high-resolution XPS spectra shown in Figure 2.3. Analysis of the XPS high-resolution spectra reveals that Mo is present both in the Mo^{6+} oxidation state, corresponding to the MoO_3 phase, with a smaller amount of Mo^{4+} state (MoO_2) in both of the post-annealed f-PLD and n-PLD thin films.

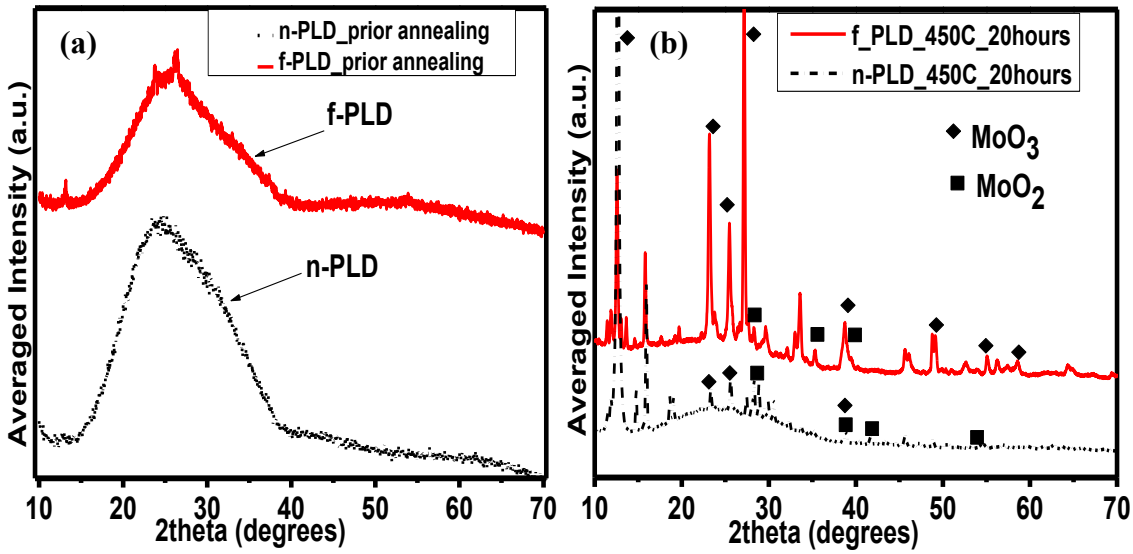

Figure 2.2. (a) Left panel- XRD patterns showing of pre-annealed n-PLD (dotted line) and f-PLD (solid line) thin films. (b) Right panel- Post-annealed XRD patterns showing n-PLD (dash-dotted line) and f-PLD (solid line) thin films and peak locations of the orthorhombic α-MoO_3 phase; the majority of the remaining peaks are attributed to the MoO_2 phase.

This somewhat of a surprising result given that no oxygen was introduced in the growth chamber during f-PLD synthesis whereas oxygen gas was used during n-PLD growth of molybdenum oxide thin films. I have found no evidence from my XPS spectra of a hydroxyl component in the Mo 3d spin orbital doublet. Further XPS studies are currently being carried out on the pre-annealed f-PLD and n-PLD films to determine whether the annealing of the thin films under atmospheric conditions may have been sufficient in replenishing oxygen and oxidizing Mo^{4+} to Mo^{6+}.

Figure 2.4 clearly shows the change of Raman band spectrum for pre-annealed samples vs post-annealed thin film samples. The highly amorphous nature of the pre-annealed n-PLD film is evident in that the high range of disorder give rise to broad-featured band in the Raman spectrum.

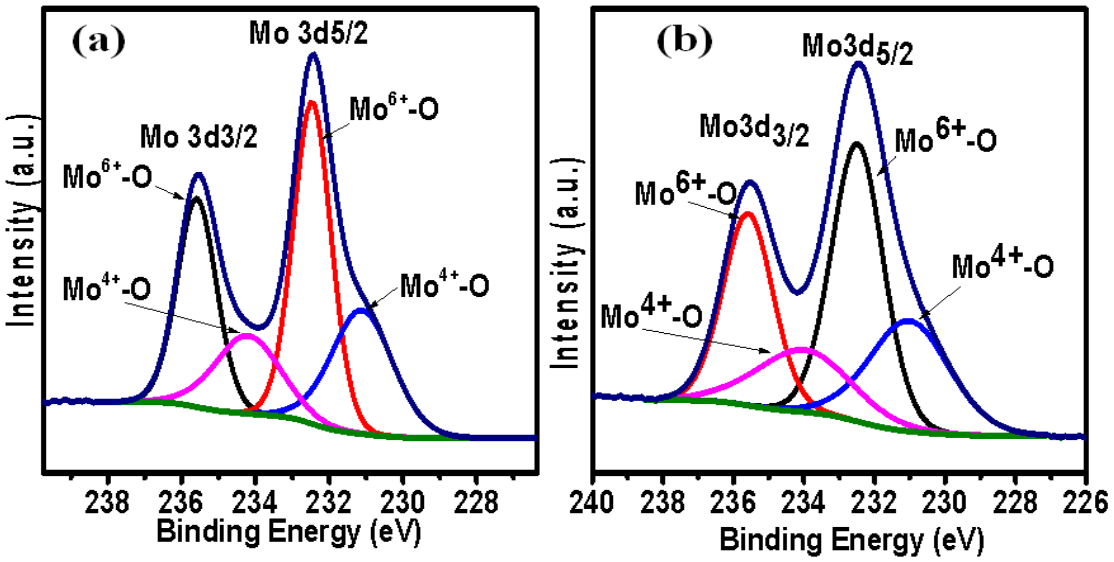

Figure 2.3. XPS high-resolution spectrum showing the fitted Mo 3d doublet peak for (a) f-PLD thin film and (b) n-PLD thin film annealed at 450 °C.

Table 2.1. Summary of fitting results of the high-resolution XPS data representing the Mo 3d spin orbital component peak parameters for the post-annealed f-PLD and n-PLD thin films. The position values are in good agreement with the work of Baltrusaitis et al. [9]. The Standard Deviation (St. Dev.) values have been estimated by performing the Monte-Carlo simulated error analysis within the CasaXPS software.

Peak type component- Mo 3d (deconvoluted)		Position (eV)	FWHM (eV)	Area	%Area	Position St. Dev. (Area St. Dev.)
f-PLD	Mo^{6+} ($3d_{5/2}$)	232.46	1.21	2593.67	31.36	0.0041 (40.6587)
	Mo^{4+} ($3d_{5/2}$)	231.11	1.96	1614.08	19.52	0.0220 (41.7210)
	Mo^{6+} ($3d_{3/2}$)	235.59	1.25	1729.11	30.28	0.0045 (27.1058)
	Mo^{4+} ($3d_{3/2}$)	234.21	2.08	1076.05	18.84	0.0250 (27.8140)
n-PLD	Mo^{6+} ($3d_{5/2}$)	232.49	1.73	2297.44	31.57	0.0048 (80.8277)
	Mo^{4+} ($3d_{5/2}$)	231.01	2.67	1411.21	19.39	0.0535 (46.4044)
	Mo^{6+} ($3d_{3/2}$)	235.59	1.66	1531.63	30.49	0.0078 (53.8852)
	Mo^{4+} ($3d_{3/2}$)	234.00	3.14	931.40	18.54	0.0500 (30.6269)

Conversely, the Raman spectra of the post-annealed films have distinct and relatively sharp bands that are consistent with the presence of both MoO_3 and MoO_2 in the thin films. The peaks at about 198, 224, 341, 356,452, 488, 566, 579, 732 cm^{-1} are

consistent with the MoO_2 bands in the spectrum with an average Raman shift of 3 cm^{-1} as compared to the study of molybdenum oxide thin films made by Camacho-Lopez et al [10].

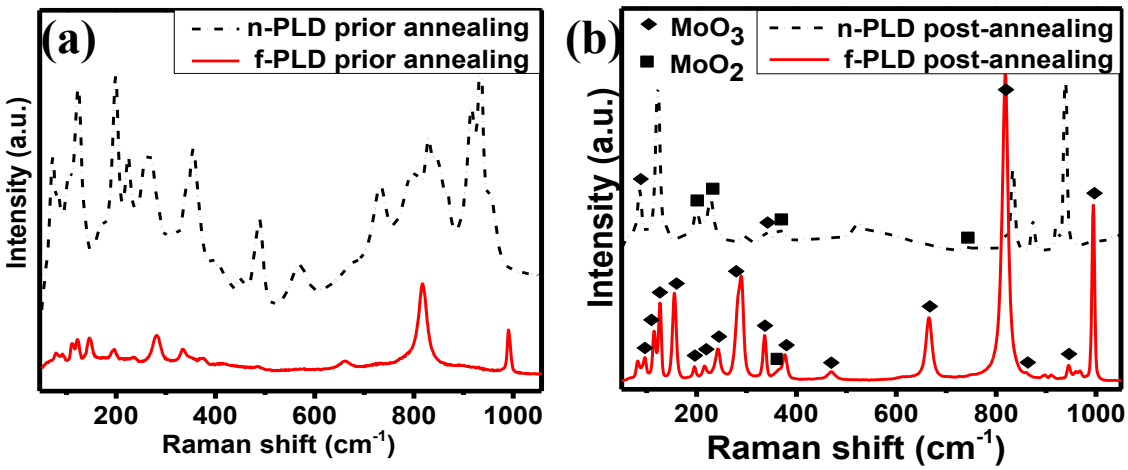

Figure 2.4. Raman spectra of f-PLD (solid line) and n-PLD thin films (dash-dotted line) (a) prior- annealing & (b) post-annealing at 450 °C for upto 20 hours.

Moreover, the f-PLD sample shows Raman peaks at 664 (B_{3g}- ν), 817 (B_{1g}-ν) which correspond to the Raman-active stretching modes of the bridging oxygens – OMo_3 (triply-coordinated oxygen), OMo_2 (doubly-coordinated oxygen) respectively and the peak at 993 cm^{-1} (A_{1g}, B_{1g}-ν) to Mo=O (terminal oxygen bond) vibrations which results from an unshared oxygen [2].

Conclusions

The f-PLD film show considerably more enhanced nano-structured texture vs the n-PLD films, prior to annealing whereas both film types exhibit highly amorphous atomic-scale structure. Oswald ripening leads to the formation of nano- to micro-sized

crystallites upon annealing in the films with a rougher morphology and smaller scale features in the post-annealed f-PLD thin film. My XRD, XPS and Raman data show that both the f-PLD and n-PLD result in an admixture of MoO_3 and MoO_2 in the thin films after annealing. Provided that further investigations on how the femtosecond laser peak power and short laser pulse duration affect the deposition of thin film material on various substrates and under varying conditions, the f-PLD technique appears to be promising for the synthesis of novel molybdenum oxide thin films.

Acknowledgements

We thank partial support from the MSU Graduate College and Rishi Patel of JVIC for XPS measurements and US Photonics for using their facilities to prepare the f-PLD thin films.

References

1. S. S. Kanu, R. Binions, *Proc. R. Soc. A* **466**, 19–44 (2009).

2. G.-A. Nazri, C. Julien, *Solid State Ionics* **53**, 376-382 (1992).

3. S.S. Sunu, E. Prabhu, V. Jayaraman, K.I. Gnanasekar, T. Gnanasekaram, *Sens. Actuators B-Chem* **94**, 189-196 (2003).

4. S. Balendhran , S. Walia , H. Nili , J. Z. Ou , S. Zhuiykov , R. B. Kaner , S. Sriram , M. Bhaskaran , K. Kalantar-zadeh, *Adv. Funct. Mater.* **23**, 3952-3970 (2013).

5. S. Amoruso, G. Ausanio, R. Bruzzese, M. Vitiello, X. Wang, *Phys. Rev. B* **71**, 033406 (2005).

6. M. Okoshi, K. Higashikawa, M. Hanabusa, *Appl. Surf. Sci.* **154–155**, 424–427 (2000).

7. M. Sanz, R. de Nalda, J.F. Marco, J.G. Izquierdo, L. Ban˜ares, M. Castillejo, *J. Phys. Chem. C* **114***,* 4864–4868 (2010).

8. J. Perriere, E. Millon, W. Seiler, C. Boulmer-Leborgne, V. Craciun, O. Albert, J.C. Loulergue, J. Etchepare, *J. Appl. Phys.* **91**, 690-696 (2002).

9. J. Baltrusaitis, B. Mendoza-Sanchez, V. Fernandez, R. Veenstra, N. Dukstiene, A. Roberts, N. Fairley, *Appl. Surf. Sci.* **326**, 151–161 (2015).

10. M. A. Camacho-Lopez, L. Escobar-Alarcon, M. Picquart, R. Arroyo, G. Cordoba, E. Haro-Poniatowski, *Optical Materials* **33**, 480-484 (2011).

CHAPTER 3: SUBSTRATE EFFECTS ON THE STRUCTURAL AND MORPHOLOGICAL ASPECTS OF MOLYBDENUM OXIDE THIN FILMS SYNTHESIZED BY NANOSECOND PULSED LASER DEPOSITION

Abstract

Molybdenum oxide thin films have been synthesized using the nanosecond-based pulsed laser deposition technique at elevated substrate temperatures resulting in the formation of sub-stoichiometric phases (O: Mo < 3) in the annealed condition on various substrates (glass slide, sapphire, Si wafer). The effects of type of substrate and the extent of annealing are studied in terms of the structural, morphological and surface chemical properties of the thin films. I find that while molybdenum oxide films deposited on both the Si and sapphire substrates had formation of nano-crystalline features upon annealing, the sub-stoichiometric deficiency was more pronounced in the MoO_x thin film deposited on Si substrate (MoO_x/Si). The morphological and structural variations among the two types of films may be due to the effects of wettability and strain-induced formation mechanisms upon deposition on dissimilar crystalline substrates. These characterization results are discussed in terms of applicability to surface related applications such as photocatalysis.

Introduction

Molybdenum oxide has been shown to exhibit characteristics promising for applications in the fields of photocatalysis [1], battery materials (both cathodic and anodic [2], electrochromic devices [3], photochromic device applications [4,5] and in gas

sensing applications [6-8]. Binary and ternary oxides of molybdenum in combination with other transition metals/ metal oxides, particularly when used as supported structures on high surface area substrates of both acidic and basic nature (e.g. alumina, silica), have the capability of working as hydrodesulphurization (HDS) catalysts [9,10]. The orthorhombic crystal structure phase has the most favorable characteristics for the above-mentioned applications. This is because of the layered, porous and intercalated aspects of the structure, which enable easy diffusion for any inserted species into the intercalation channels. However, polymorphs of this oxide, namely, a metastable β-MoO_3 with a monoclinic crystal structure, which is similar to a distorted rutile-type atomic arrangement, also exists both in the bulk [11] as well as in nanoscale materials [12]. This metastable structure transforms to the thermodynamically stable α-phase at temperatures above 350 °C [12]. Additionally, several sub-stoichiometric oxides of the general notation: Mo_nO_{3n-1}(where, n = 4, 5, 8, 9, 10, 17, etc.), have also been studied [13-15]. In any of these oxygen-deficient phases, the ratio of Mo:O varies between: 2.75-2.91 [14]. The Mo_4O_{11} sub-oxide has monoclinic(η) and orthorhombic (γ) variants, all of which form only after a threshold of oxygen concentration is reached under equilibrium conditions [16]. On the other hand, molybdenum dioxide (MoO_2) is also a well-established battery (anode) material having a monoclinic, distorted-rutile type structure [17,18] and possessing metal-like properties [19]. In addition, the amorphous molybdenum (a-MoO_3) oxide thin films have some interesting photochromic properties compared to the above mentioned crystalline phases, hence making them industry viable components [20]. The structure and properties of molybdenum oxide based thin films can be altered extensively by changing the parameters of deposition in chemical vapor

deposition (CVD) or in physical vapor deposition (PVD) [21]. Nevertheless, issues of obtaining stoichiometric MoO_3 thin films can arise from multiple effects, understanding of the effect of deposition conditions of any specific film synthesis technique can help us produce the desired composition, structure and properties of such transition metal oxides. In particular, PLD has the unique capacity to produce metal oxide thin films in a reactive gas atmosphere at low temperatures having a prescribed stoichiometry and high crystallinity. More often than not, the nanostructured morphology of molybdenum oxides has much better applicability and superior properties when compared to its meso-/ micro-sized counterparts. Conversely, an accurate control of the various sub-oxides of the molybdenum can also lead to unique and novel electrical and optical properties which can be correlated to better photocatalytic activity [16]. Hence, the current need in terms of parametric control in PLD technique requires a full understanding of the effect of the substrate-thin film interaction upon deposition and under annealing conditions.

An extensive characterization study of nanosecond-laser based PLD (n-PLD)-made molybdenum oxide thin films (MoO_x) deposited on single crystal substrates (both Si-wafer and c-plane sapphire), in terms of the structural, surface chemical and morphology of the thin films primarily after annealing, is presented herein. The results are explained in terms of the creation of multivalent states of Mo, and their potential cause of origin, and the effects imposed upon by the substrate during the deposition and during annealing of the thin films.

Experimental Details

The Molybdenum oxide thin films were synthesized using pulsed laser deposition (PLD) MoO_3 targets using commercially available pure MoO_3 powder (99.97 %, Fischer-Scientific). Upon finely grinding and homogeneously mixing the powder with PVA, the material was then pressed using a 10 Metric Ton hydraulic press. The smooth, powdery pellets that were thus formed were subsequently sintered in air at about 650 °C for at least 12 hours in a muffle furnace. A compact and well textured orthorhombic phase MoO_3 target was confirmed using x-ray diffraction (XRD) and subsequently employed in the PLD chamber.

Thin films were synthesized on microscopic glass slides (Corning-25 x 25 mm), polished sides of silicon (Si) wafer (<100> n-type) substrate and c-plane (0001) sapphire substrates, all done at elevated substrate temperature. Substrate cleaning was made in a three-step process as follows: ultrasonic cleaning in Acetone (10 minutes), Ethyl Alcohol rinsing and finally thoroughly rinsed in DI water and air dried. Immediate placement of the substrates in the vacuum chamber and heating of the substrates (T_s = 300 °C) was made in order to minimize the surface overexposure to hydroxylation. After attainment of the desired substrate temperature under vacuum in the deposition chamber, where the temperature was monitored using a thermocouple and controlled using a temperature controller, the oxygen atmosphere was established to stabilize the reactive atmosphere. The deposition chamber was consistently evacuated to an initial base vacuum of 10^{-5} mbar (10^{-3} Pa) initially and then pumped back with oxygen gas (>99%, Airgas) up to one order magnitude increase in the chamber pressure gauge reading (10^{-4} mbar, or 10^{-2} Pa). The laser source used for PLD was a nanosecond (ns) pulsed UV-excimer based KrF

laser with $\lambda = 248$ nm and pulse duration of ~ 20 ns (Lambda Physik, COMPEX201). While an average per pulse energy of 325 mJoule was employed, an energy density/ laser fluence of ~20 J/cm^2 was achieved at the target surface. The angle between the incident laser beam and normal to the target surface was maintained at 45°. Constant rotation of the target carousel (10Hz) was employed to avoid local heating of the surface, hence leading to homogenous plasma creation. With a target to substrate distance of ~6.5 cm, the measured thin films' thickness in the as-deposited condition on various substrates varied between 40 – 50 nm. All of the thickness measurements were performed ex-situ using a Veeco Dektak 150 surface profilometer, and the measurement/data analysis methods of which are discussed in the ensuing Supplementary Information section(SI).

The scanning electron microscopy (SEM) imaging and complementary energy-dispersive x-ray spectroscopy (EDX) analysis were performed on specimens of the thin films as deposited on the substrates, which were affixed to either carbon (C) or copper (Cu) tape. The SEM and EDX analyses were performed at various film locations using horizontal and tilted stage modes. For this purpose, a FEI Quanta 200 SEM instrument was employed with operating voltage of 5-20kV and an Oxford Instruments INCA EDX detector was utilized for elemental analysis. In addition to the SEM analysis, imaging of the surface morphology of the films was also made using an Atomic Force Microscope (Bruker-Dimension Icon). The single crystal (n-doped) silicon AFM probe with a radius ~8 nm (spring constant: 48 N/m and resonant frequency: 190 KHz) were used in tapping mode for these studies. The AFM data were processed using the Bruker NanoScope Analysis Suite 1.30.

Ambient temperature X-ray diffraction (XRD) measurements were performed on the thin films for structural and phase determination in both as-deposited and post-annealed conditions using a Cu-Kα radiation X-ray source (Bruker D8 Discover) with λ=1.54184 Å. The instrument parameters for the X-ray source were consistently set at 40kV accelerating voltage and 40 mA of electron current. A Gobel mirror was employed in the incident side and 0.6mm slit were used for both primary and secondary divergence slits.

The X-ray Photoelectron spectroscopy (XPS) technique was made using a twin-crystal monochromatic Al-Kα source with characteristic energy of 1486.6 eV. A Thermo Scientific Alpha 100 hemispherical Constant Analyzer Energy analyzer (CAE) with 25 eV pass energy was employed for data acquisition. The Ag $3d_{5/2}$ (FWHM=0.36 eV) peak with a characteristic energy of 368.26 eV was used for calibration of the Instrument source and analyzer. Data analysis and spectral peak deconvolution was performed using CasaXPS 2.3.16 software package, with the Marquardt–Levenberg optimization algorithm. Data calibration was performed using an internal standard-based C1s peak position referenced at binding energy (BE) 284.8 eV. A Shirley background was used for all the spectroscopic regions analyzed. Additionally, a choice of line shape between a Gaussian- Lonrentzian product, GL (30) and a Lorentzian asymmetric functional form convoluted with a Gaussian function, LA(a,b,n) was made for both the survey and high-resolution spectra. The vibrational phonon modes were determined by using a vertically polarizable green laser, λ=532 nm (Horiba LabRAM HR) based micro-Raman spectrometer having an instrumental resolution of ~1 cm^{-1} with variable optical density

filters. The Raman data was acquired and analyzed for peak deconvolution and fitting using Labspec 5 software.

Results and Discussion

It was pointed out that a variation of thermal and lattice mismatch is possible among thin films grown on different substrates, based on their respective thermal expansion coefficients and preferred orientation [22]. This in turn affects the thin film's morphology and crystal structure. Moreover, the as-deposited thin films on glass were observed to be light blue in color, which transformed as the thermal treatment was proceeding through various color stages as follows: dark bluish followed by foggy white and finally more transparent at the selected annealing temperature (450 °C). These color transitions, which are indicative in amorphous molybdenum oxide thin films, were also observed by others in their annealing studies [23]. Numerous studies have reported on the effect of oxygen partial pressure (P_{O2}) and substrate temperature (T_s) on the stoichiometry and phase purity using related techniques, such as PVD or sputtering [24, 25]. It has been reported that in-situ thermal annealing by use of the heated substrate has a pronounced effect on the extent of crystallinity of the as-deposited thin films [21]. In addition, the chamber pressure directly affects the grain size of the thin films during deposition [26]. Moreover, the thermal annealing of the post-deposited thin films typically produces more crystalline films and larger crystalline grain size, due to thermal activated atomic diffusion and Ostwald ripening, respectively. The enhanced diffusion and greater tendency of the atoms to organize in crystalline arrangements also leads to more enhanced atom-to-atom interactions with crystalline substrates at higher annealing

temperatures [27]. XRD analysis of the as-deposited thin films on all three types of substrates shows these to be highly predominantly amorphous in nature (see, for example, Figure 2.1a in Chapter 2 and in the Supplementary Information (SI) section.

The change from amorphous to crystalline nature is likely dependent on the thickness of the thin films. The SEM images and film thickness measurements show evidence of non-uniform thickness in all of the thin films synthesized for this study. As discussed below, the non-uniformity appears to be of importance in the inhomogeneity of the crystalline regions upon annealing of the thin films.

For the film deposited on the Si substrate (MoO_x/Si thin film) at a substrate temperature (T_s) of 300 °C after ex-situ annealing at 450 °C for 6 hours, as shown in Fig. 3.1(a), the development of granular texture was obtained in some regions owing to the crystalline rearrangement during thermal treatment. This is consistent with the XRD results (shown below) showing that an orthorhombic structure has developed along with an amorphous component in the MoO_x/Si thin film Interestingly, there were additional regions with micro-nano crystallites observed in the SEM images, (width $<<$ 1 μm; several microns in length) having faceted features. A folded-like texture was also predominant in major areas of the post-annealed thin films. Interestingly, there were some regions consisting of mixed amorphous/crystalline phases, which could be best described as crystalline phases embedded in an amorphous matrix. In addition, there were also regions of different grain shapes ranging from needle-like to ellipsoidal, including elongated columns. The resulting morphology may be due to an insufficient annealing time (6 hours) provided for the larger areas of the thin film's surface. On the other hand, the formation of molybdenum oxide(s) having this varied morphology in the MoO_x/Si

thin film, which suggests presence of primary and secondary phases, may also result from the annealing process. In addition, the effects due to ionizing radiation causing material change and modification cannot be fully discounted. Earlier reports have shown evidence of partial transformation of the MoO_3 to MoO_2 through ion bombardment upon major irradiation from X-rays or electrons, which are present in any characterization study vis-à-vis SEM, XRD, XPS [28].

Attempts at scraping of the thin films showed a high level of adhesion for the as-deposited MoO_x/Si thin film. This is most likely due to the formation of covalent bonding between the MoO_x thin film and the Si/SiO_2 substrate. Apart from this, an observation from the morphology that may reflect upon the crystallite growth or deposition mechanisms is worth mentioning. I observed circular-shaped predominantly amorphous regions containing some segregated crystallites with globular-type craters in the middle. Lopez et al observed similar distinguishable annular craters in their laser-induced structural transformation study of molybdenum oxides [19].

The SEM images of the post-annealed thin film (450 °C-6 hours) deposited on sapphire substrates (Fig. 3.1 (c, d)) show a much more uniform coverage than the film deposited on Si. This suggests a higher wettability of the film deposited on sapphire (MoO_x/sapphire) compared to the film deposited on Si. I conjecture that this greater wettability may be associated with a tendency of the crystallites of the thin film to form epitaxial registry, although with considerable lattice mismatch, with the sapphire substrate. This is consistent with several features observed in the post-annealed thin film, such as ruptures and micro cracks that developed in dendritic-like pattern. SEM imaging of the regions containing the micro-cracks proved to be difficult due to substantial

charging effects associated with the sapphire-exposed areas. The lower wetting mechanism of the thin film on the Si substrate, which results in a large contact angle between the film and substrate, is also consistent with the formation of globule-like regions and in the greater tendency of retaining semi-crystalline or mixed amorphous/crystalline character upon annealing.

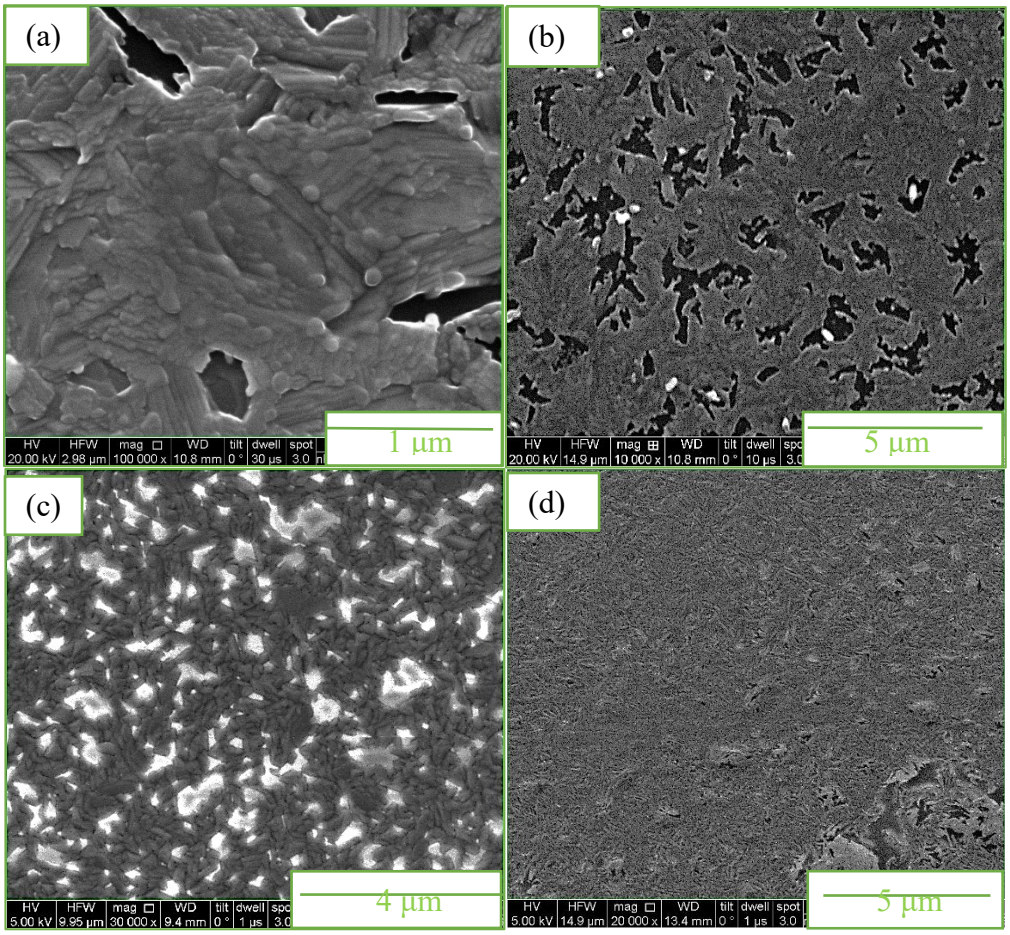

Fig. 3.1. SEM micrograph of MoO_x thin films deposited on the Si substrate (a & b), and sapphire substrate (c & d), both annealed at 450 °C for 6 hours (at various magnifications).

Because of the incomplete transformation of the amorphous regions when compared to post-annealed thin film on the sapphire substrate, another annealing cycle was performed on the MoO_x/Si thin film for an additional 6 hours. SEM images of the

thin film exposed to the second annealing cycle revealed excellent terraced- crystallites (Fig. 3.2 (a)), owing to the additional nucleation and growth due to Ostwald ripening. The morphology of tabular, elongated crystallites is consistent with the orthorhombic phase-type growth of MoO_3 (see Fig. 3.2 (a, b)). In all, there was an admixture of crystalline orthorhombic-like phases with an amorphous moiety extending throughout the film. In addition, there are smaller more roundish nanoscale features, which are consistent with additional thermodynamically stable MoO_x phases: As shown in the following discussions, this is consistent with the XRD characterization of the thin films.

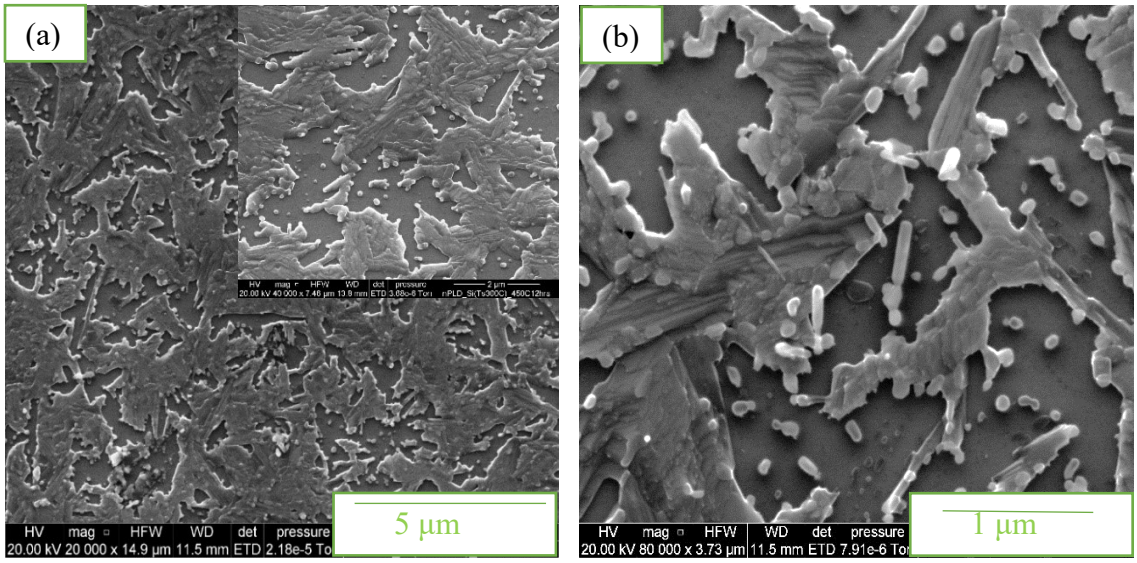

Fig. 3.2. (a) SEM image of MoO_x/Si thin films after annealing for a total of 12 hours, shows development of terrace-like features on a large scale (the inset is of a tilted scan close-up image (tilt angle-30°) justifying the clear faceting aspect in a step-like nature, 2 µm scale). (b) some regions also possessed highly strained, rod-like feature in combination with the faceted planes.

Almost all of the post-annealed samples varied considerably in appearance (see SI) with respect to their as-deposited counterparts, in the sense that they had a foggy, translucent character, which might be related to their larger grain size. Comparatively, the

MoO_x thin film deposited on sapphire had more densely packed nanograins than the molybdenum oxide film deposited on the Si substrate.

After extensive annealing (for 20 hours at 450 °C) of the molybdenum oxide thin film deposited on the glass substrate (MoO_x/glass; T_s = RT), SEM images (see Fig. 3.3) revealed the growth of slabs of nano- to micrometer-extent having nanometer thickness, stacked along their rectangular regions forming a series of cascades. This behavior was also nominally observed in the molybdenum oxide thin film deposited on Si. Extreme faceting of the larger areas was observed owing to the anisotropic growth during longer annealing times (20 hours) on the MoO_x/glass thin film.

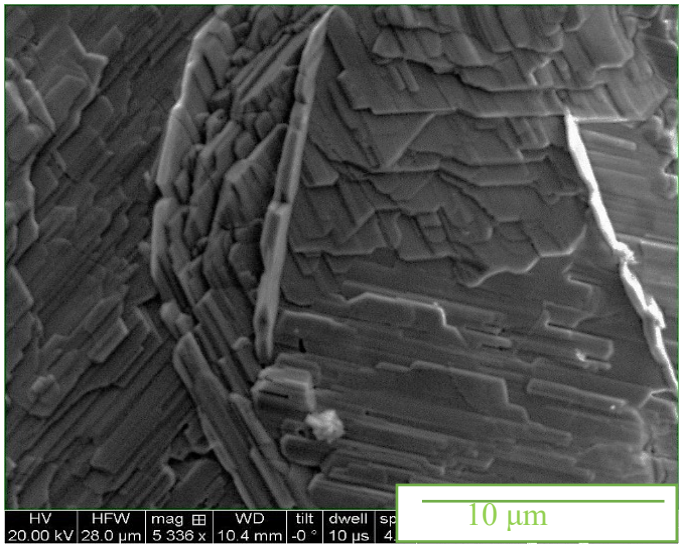

Fig. 3.3. SEM micrograph of post-annealed thin film (for 20 hours) deposited on the glass substrate (n-PLD, T_s=RT).

The AFM imaging has been very useful for providing information on the aspect ratio of the thin film samples along with textural information in terms of the film surface roughness (R_{rms}). As it is clearly evident from Fig. 3.4, the post-annealed thin film deposited on the Si substrate has more elongated nanocrystals along with a wider range of

crystallite sizes (starting from at least ~70 nm) than the post-annealed MoO_x/sapphire thin film.

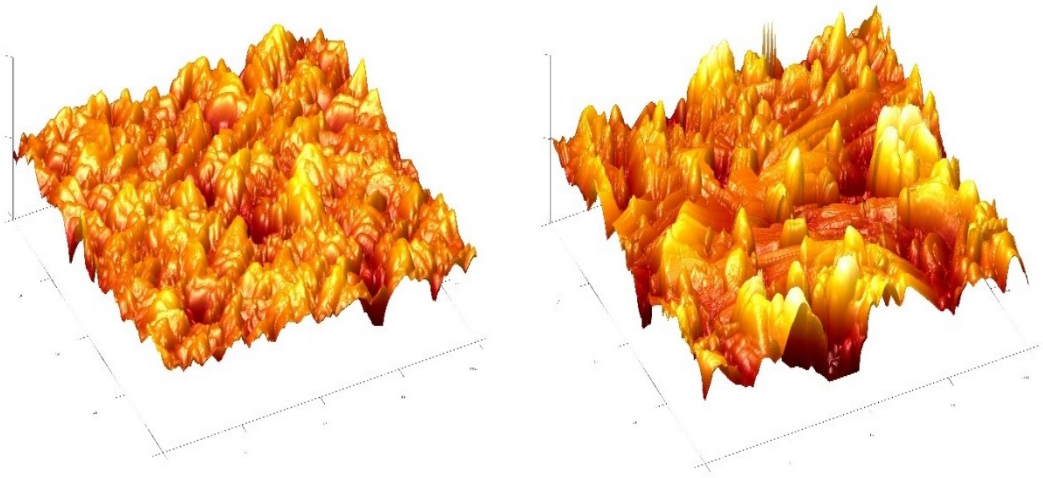

Fig. 3.4. AFM 3D images of post-annealed samples of MoO_x thin films on: sapphire substrate (left) with the depth (z-axis) of 41.1 nm and Si substrate (right) with the depth (z-axis) of 81.4 nm. The scale bar in the xy-plane is 2 μm x 2 μm.

Moreover, when viewed in combination with the SEM micrographs shown earlier (Fig. 3.1 and Fig. 3.2), it can be surmised that the thin film deposited on Si favors the creation of a multilayered morphology; however, the multilayering is considerably more pronounced in the MoO_x/glass thin film.

A more densely packed grainy texture is observed in thin film deposited on sapphire in comparison to the one deposited on Si, from the nanometer-scale particle analysis of the AFM 2D image (Fig. 3.5 (a, b)). If observed carefully, there were interference hues throughout the 2D image of MoO_x/Si (Fig. 3.5 (b)). This might be due the semiconducting nature of the substrate. The roughness factors (Rq), which are calculated using AFM 2D micrograph analysis are ~13 nm for MoO_x/sapphire in comparison to the ~23.2 nm for the one deposited on Si (MoO_x/Si). Thus, the Rq for

MoO_x/Si thin film is ~76% higher than that of MoO_x/sapphire thin film, despite the Si-substrate being considerably smoother than the sapphire substrate. This effect has been explained by Illyaskutty et al [22], who claim that smoother substrates have lower adhesion irrespective of the nature of the film-substrate bonding mechanism (Van der Waals attractions, Chemisorption etc.).

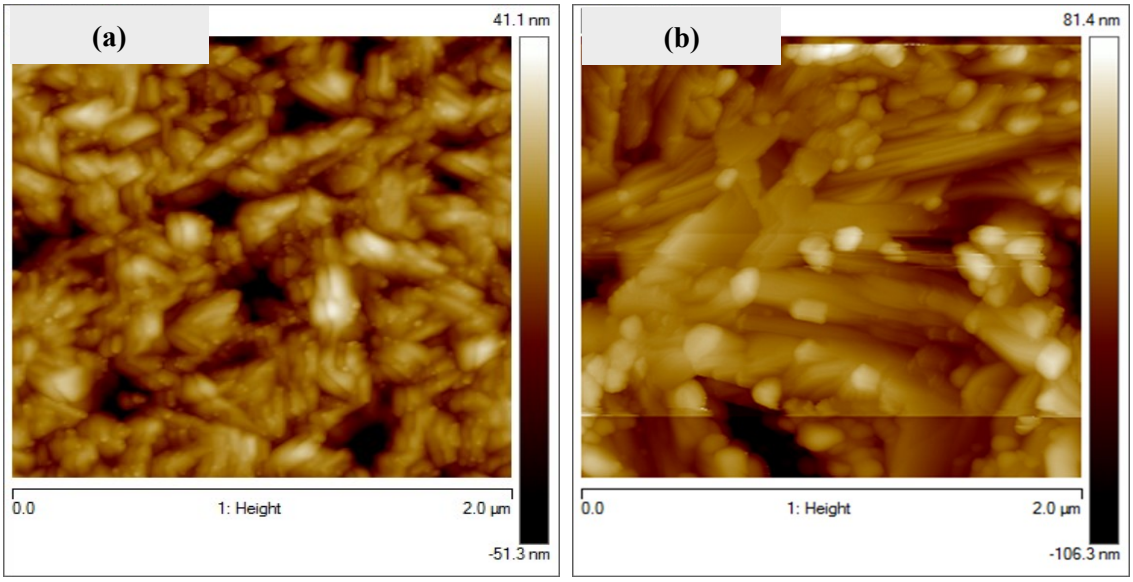

Fig. 3.5. AFM 2D images (2 µm x 2 µm) of post- annealed thin film samples of MoO_x deposited on (a) sapphire substrate (b) Si substrate.

The variation of average d-spacing suggests a less perfectly ordered system at the atomic scale whereas a fewer number of reflections/peaks in an XRD pattern is suggestive of preferential orientation of the thin film on a substrate. The preferential orientation of the nano- to micro-crystalline grains was present in both films as confirmed through phi and chi scans performed with the diffractometer. It was noted above that thin film XRD data analysis can be more challenging when compared to powder diffraction, due to preferred orientation issues in thin films which causes some of the peaks to absent from the XRD pattern.

In the analysis of the XRD data, the effects due to potential epitaxial type registry of film to substrate needs to be borne in mind. A simple calculation of epitaxial mismatch (% *l*) of the thin films with respect to their substrates, can be performed as follows,

$$l = \left[\frac{as - af}{af} * 100\right] \%$$

where, a_s and a_f are the unstrained lattice parameters of the substrates and the respective thin films, i.e. in their intrinsic state [22]. This attempt at epitaxial preference forces the film's crystal lattice to undergo a strain, which would in general be relaxed during a thermal treatment process. It should be noted that, despite the extent of epitaxial mismatch of the MoO_3 crystal lattice with the sapphire substrate being much less when compared to the silicon substrate, the residual stress/strain produced would not be the driving mechanism for any potential oxygen vacancy formation. As was mentioned above, the scraping tests performed on the as-deposited samples showed strong adhesion of the film on the sapphire substrate, partly owing to the atomic interlocking of the MoO_x crystal lattice with respect to the sapphire lattice in the c-plane, and partly due to the higher degree of wettability of the MoO_x/Al_2O_3 interface.

Added to this, the effect of thermal conductivity and thermal expansion coefficients can also significantly override the natural growth of thin film on these substrates. For example, as per the work of Illyaskutty et al [22], since the thermal conductivity of Si is more than 200% greater than that of sapphire substrate, this substantially impacts grain growth propagation throughout the substrate surface when uniformly heated during annealing. Coincidentally, the effect due to this thermal conductivity difference has been observed in the morphological differences of the thin films, i.e., MoO_x/Si shows elongated layered structures, which is related to the enhanced

thermal conductivity of Si. At the same time, the sapphire substrate, despite being more epitaxially suitable, provides lower mobility for the growing crystallites, hence hampering the creation of the desired morphology during annealing.

Upon analysis of the MoO_x/Si thin film XRD pattern shown in Fig. 3.6, I find evidence for a pseudo-amorphous component from the peak centered at ~16° and a η- and/or χ-Mo_4O_{11} component in the thin film: Note that the background, which shows additional evidence of an amorphous component, has been partially removed from the XRD pattern. The Mo_4O_{11} phase has a dimension that is particularly small in the nanoscale, as evidenced from the peak at 22.64°. This is due to the extreme variation in the confinement aspect of the scattered X-rays in the diffraction experiment being very small for one set of planes versus the preferentially oriented planes of the elongated nano-crystallites, which in turn causes broader than usual peaks based on the Scherrer relationship of FWHM and the crystallite size. Thus, it is evident that a mixture of MoO_3, Mo_4O_{11} and potentially other MoO_x phases persist in the thin film deposited on the Si substrate. Moreover, XRD measurement of molybdenum oxide structures on Si-based supports is very challenging because of the high intensity of the Si peak coinciding with the 2θ positons of molybdenum oxide phases. The solution for this is by employment of chi angle and phi angle scans. This allows for the reduction of the single crystal silicon's intense peak, and simultaneously improving the count statistics for measurement of the thin film's diffraction pattern. The precise determination of the amorphous component of the thin film on Si substrates, say by use of Rietveld refinement, is complicated due to an amorphous SiO_2 or SiO oxide layer on Si [29]. It is because of such complexities that I chose not to perform Rietveld refinement of the XRD data measured from the thin films.

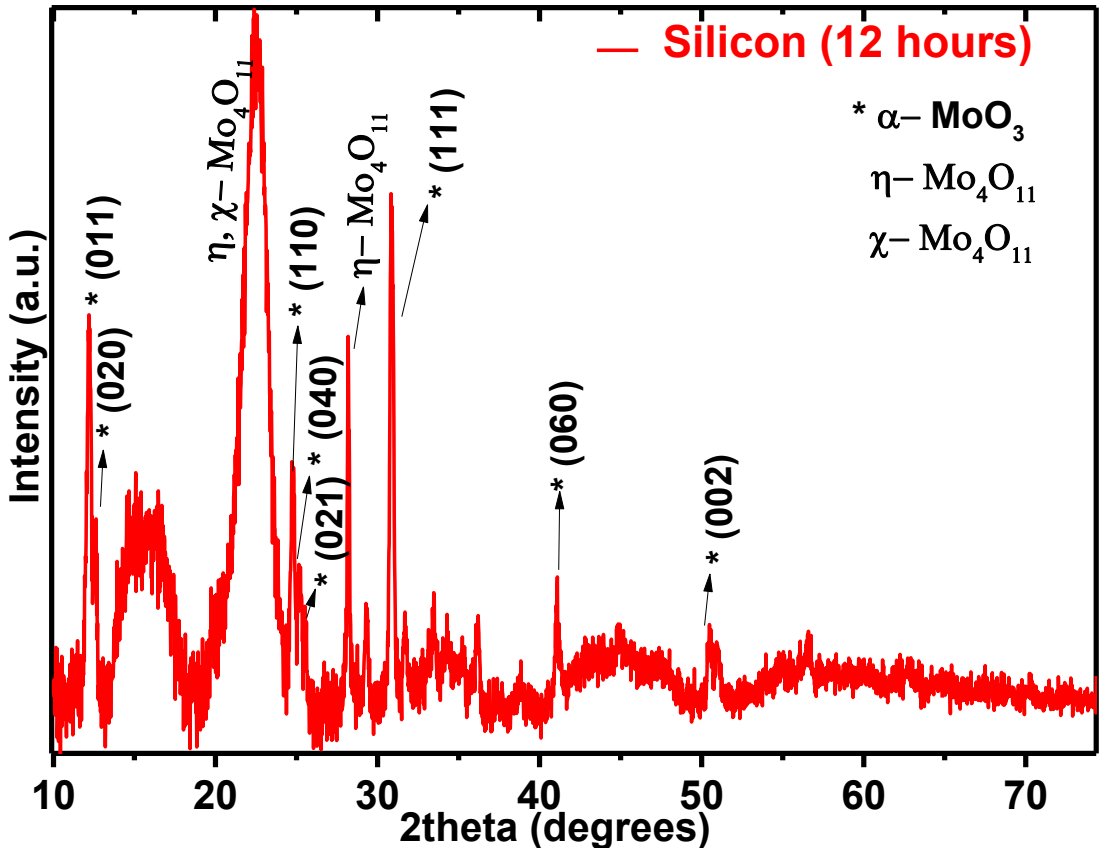

Fig. 3.6. Typical XRD pattern of the MoO_x/Si thin film after thermal treatment (450 °C-12 hours). The inset shows the pseudo-amorphism from the shorter atomic planes.

The MoO_x thin film deposited on the sapphire (c-plane) substrate (MoO_x/sapphire), has been shown to develop a highly epitaxial nature based on the domain matching epitaxy mechanism, which corresponds to the matching of lattice planes of same or multiple integral nature [16]. As can be seen in the diffraction pattern shown in Fig. 3.6 and as is the case for the MoO_x/sapphire thin film (Fig. 3.7), the identified peaks show that a mixture of MoO_3, Mo_4O_{11} and potentially other MoO_x phases are present in the MoO_x/sapphire thin film.

Moreover, the MoO_x/sapphire thin film exhibits d-spacing shifted to slightly lower 2θ values in relation to that of the MoO_x/Si thin film. It is plausible that this is due to the epitaxial mismatch difference being considerably lower for MoO_x vs sapphire than of MoO_x vs Si, for their respective lattice plane orientations at the thin film-substrate interface.

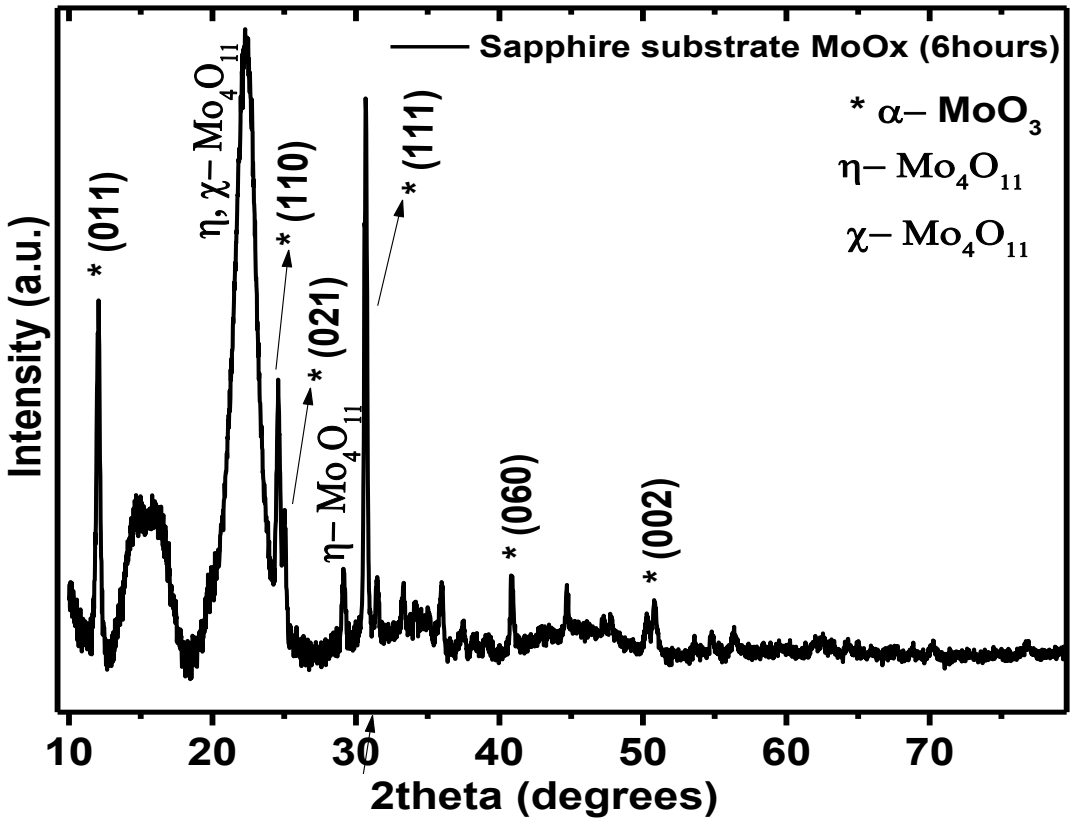

Fig. 3.7. XRD pattern of the MoO_x/sapphire thin film after thermal treatment (450 °C-6 hours).

The chemical states of the thin film surfaces were probed using XPS, both through survey spectrum and high-resolution (HR) scan analysis. The XPS spectra collected from the MoO_x/sapphire thin film showed evidence for hydroxide formation most likely due to a nominal hydroxylation of the sapphire surface's dangling bonds at

the oxygen sites. The survey scans measured from all of the films showed, in addition to peaks from Mo and O, signal that originated from the substrate material (e.g., Si for Si substrate, Al for glass and sapphire substrates, etc.). The XPS analysis of the thin film deposited on the glass substrate has been discussed in Chapter 2. Based on the analysis of the XPS survey scan (Table 3.1 and Fig. 3.8) and high-resolution spectra of O1s and Mo3d (Fig. 3.9 and Table 3.2), it can be postulated that an admixture of the hexavalent (Mo^{6+}) and a combination of pentavalent (Mo^{5+}) and the tetravalent (Mo^{4+}) was present, which was modeled using an admixture peak labeled as Mo^{x+}, is evident in the MoO_x/sapphire thin film. The stoichiometric ratios of O: Mo were calculated starting with an elemental quantification of all possible atomic concentrations from the survey scans and employing all possible oxidation states in the high resolution scans of Mo 3d. The mixed-oxide phase is predominantly in the Mo^{6+} state and only ~ 10.39 at% accounts for the mixed pentavalent and tetravalent mixed oxide state.

Table 3.1 Summary of the XPS survey scan elemental quantification measured from molybdenum oxide the thin film on the sapphire substrate. The atomic concentration data (at% conc.) along with the Standard Deviation (% St. Dev) has been obtained by using a Shirley background.

Name	Position	FWHM	Area	at% Conc.	% St.Dev.[1]
O 1s	530.56	1.895	6000.99	64.39	0.502
Mo 3d	232.56	1.873	5689.35	18.83	0.213
Al 2p	74.56	1.532	286.67	16.78	0.582

[1] Standard deviation of the % Atomic concentrations of each of the elements.

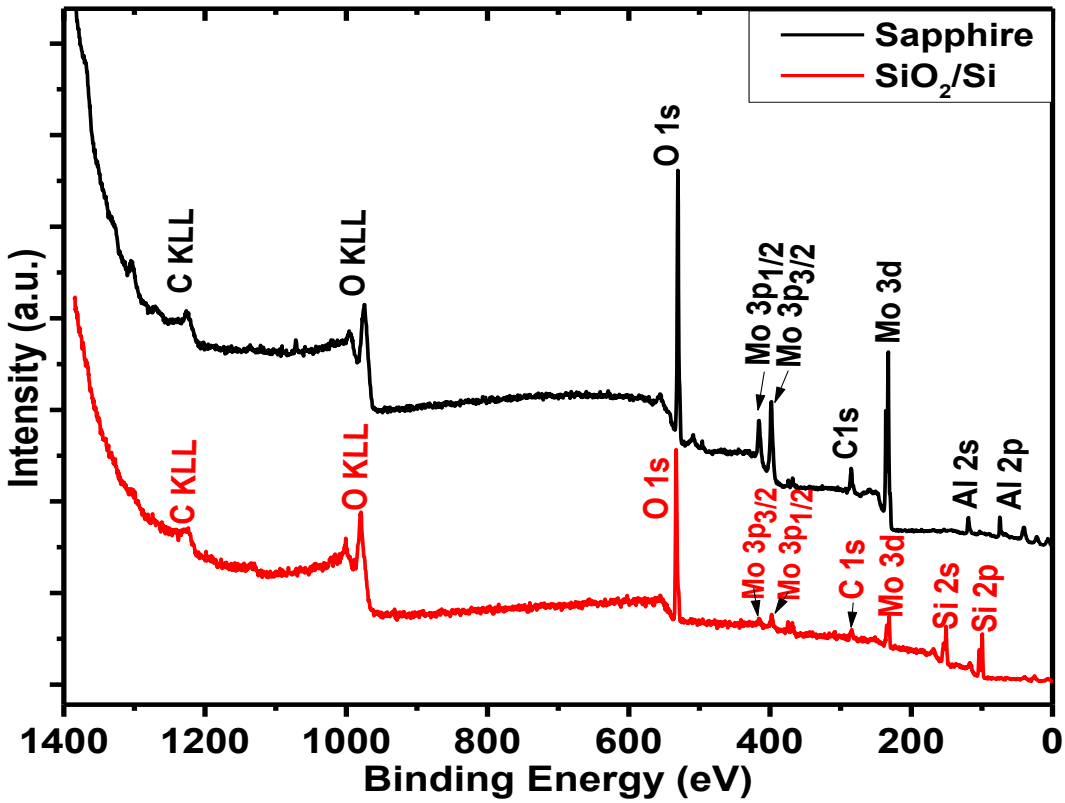

Fig. 3.8. The survey scans of thin films on both the substrates: sapphire (Black-Top) and Si (Red-Bottom) showing the presence of only the constituent elements present in the thin films (Mo, O) and substrates (Al from sapphire; Si from silicon substrate).

Moreover, it has been pointed out that these sub-oxides possess the largest values of FWHM among all possible oxides of molybdenum, partly owing to the reason that there were at least 7 noted sub-stoichiometric oxides of varied MoO_x phases [15]. Upon calculating the elemental at% concentrations from the survey scans, and accounting for the Al-O (Al_2O_3) bond component in the O1s HR spectrum, it was concluded that the relative O: Mo was ~2.9. The accurate estimation of all the sub-oxides along with their atomic concentrations would warrant a higher spectral resolution in the HR scans, which was a serious limitation to this experimental procedure, even after optimization of the fitting parameters. The results from fitting of the high-resolution spectra of the Mo 3d

and O1s regions were found to be in conformance within my constraint method (Fig. 3.9).

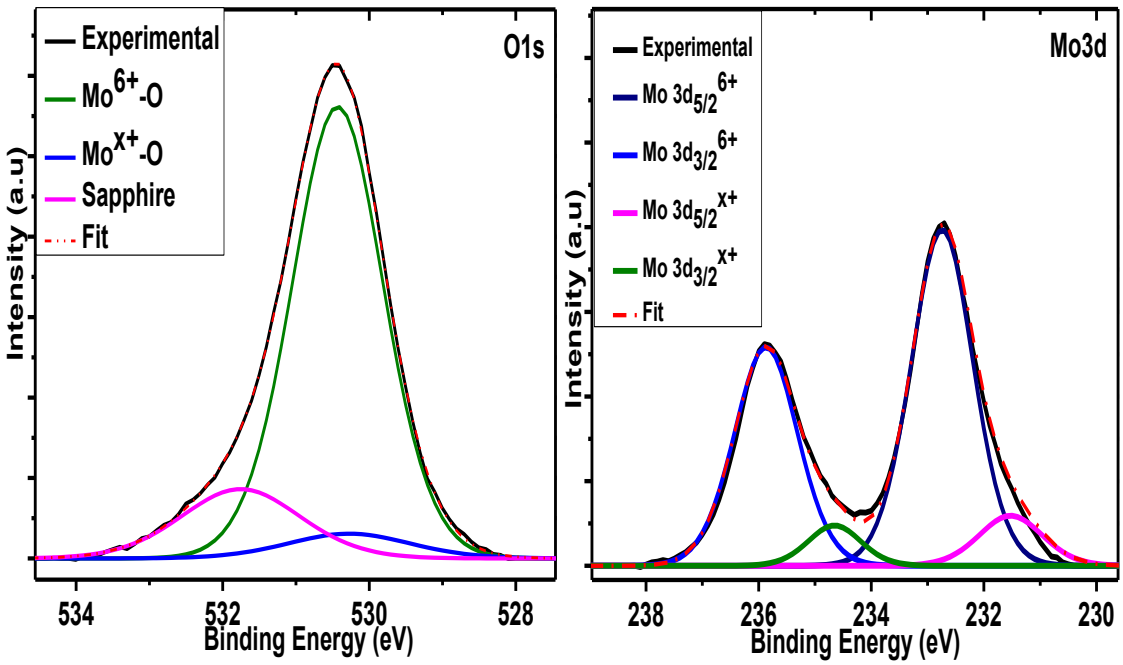

Fig. 3.9. The high-resolution (HR) spectra fitting of MoO_x/sapphire thin film showing O1s (left) and Mo3d (right) components. The fitting parameters and constraints are partly based on the output from the survey scan regarding the possible components and their corresponding peak positions. The fitting summary is detailed in Table 4.1.

While the HR XPS spectra measured from the MoO_x/Si thin film did not have any major charging features, which is reasonable based on the semi-conducting nature of Si, there was a significant distortion in peak shape of O1s HR spectrum. As shown in Fig. 3.10, the lower binding energy (BE) feature is due to the Mo-O bonding in a multivalent state, while the Si-O contribution, due to a few monolayer thickness of SiO_2 on the surface of Si, occupies the major portion of the area of the HR spectrum. There are different possible explanations for this peculiar behavior.

Besides showing presence of Si, the survey spectrum (Fig. 3.8) of the MoO_x/Si thin film shows presence of Mo and minor quantities of contamination by Ag (<2 at%). The Ag is shown to be present in either AgO or Ag_2O form, consequently adding to a slightly higher O1s at% than would be expected. A similar calculation approach, as that made for the MoO_x/sapphire thin film XPS data, was followed for the calculation of the atomic concentration ratios of O: Mo: Si from the survey scan (see SI).

Table 3.2. Summary of fitting results of the high-resolution XPS spectra measured from MoO_x/sapphire thin film. All the peak components were fitted with a Line shape based on Gaussian-Lorentzian product formula, GL (30) where the percentage of Lorentzian peak shape is indicated in the parenthesis. The standard deviation of peak areas calculated from 400 individual spectra was generated by Monte Carlo simulation-assisted peak analyses utilized within the CasaXPS software.

HR Spectrum type	Component peak	Position	FWHM	Area	%Area	%Area St. Dev.
Mo 3d	Mo^{6+} $3d_{5/2}$	232.73	1.307	2812.74	53.76	0.201
	Mo^{6+} $3d_{3/2}$	235.86	1.342	1876.1	35.85	0.134
	Mo^{x+} $3d_{5/2}$	231.5	1.147	326.133	6.23	0.170
	Mo^{x+} $3d_{5/2}$	234.63	0.974	217.531	4.16	0.134
O 1s	Mo^{6+} - O	530.43	1.47	4474.17	78.52	1.520
	Mo^{x+} - O	530.28	1.967	328.428	5.76	1.140
	Al - O (Al_2O_3)	531.76	1.918	895.233	15.71	1.38

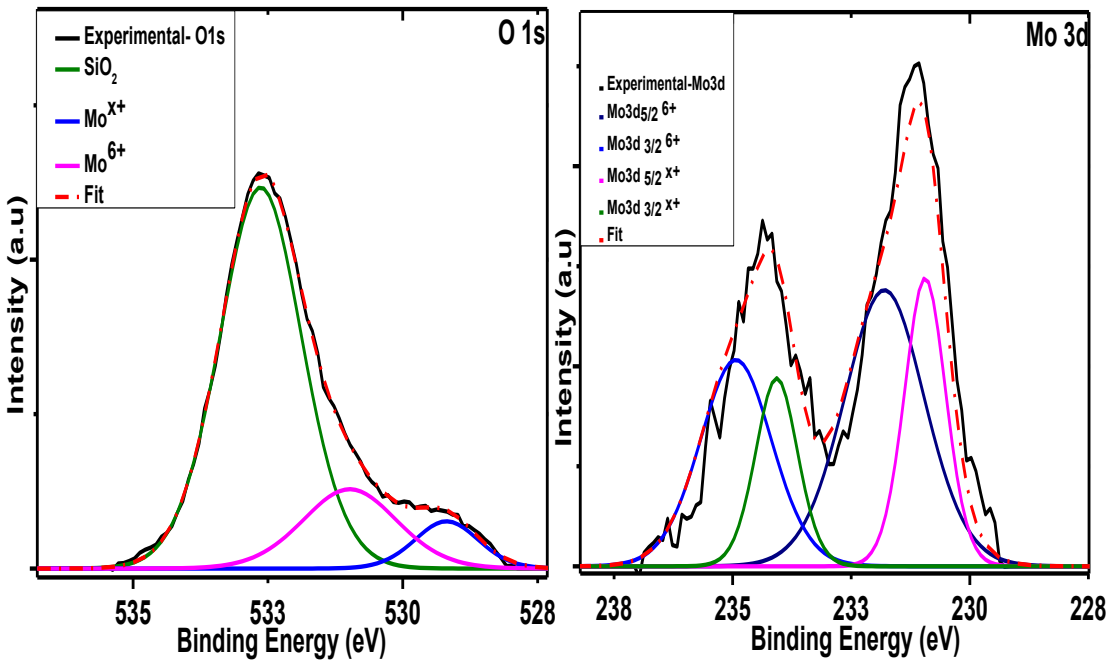

Fig. 3.10. XPS high-resolution (HR) spectra fitting of MoO_x/Si thin film with corresponding O1s (left) and Mo3d (right) component. The fitting parameters and constraints are based partly on the output from the survey scan regarding the possible components and their peak positions.

After accounting for ~24.5 at% of Si2p signal from SiO_2, an equivalent oxygen at% was removed to account for only the O: Mo ratio in the thin film. Owing to this SiO_2 (Si-O) bond constituent in the HR scan of O1s, the calculated O: Mo was ~2.84. Whereas this is consistent with the quantified values of Mo^{6+} vs Mo^{x+}, it is plausible that there are cation vacancies in the film or that extra hydroxyl components from the surface or the film/substrate interface may have contributed to the overall XPS signal [30]. While there was no hydrogen introduced to the chamber during deposition of the thin film or exposure made to a reducing atmosphere during the annealing cycle, the possibility of cation vacancy formation is peculiar only to the MoO_x/Si thin film. Moreover, the shift of the O1s peak consisting of Mo-O and Si-O components can be attributed to many known

physical phenomenon like extra-atomic relaxation due to higher amount of defects or local charging effect of the insulating type of thin film [31].

Based on the analysis of the Raman spectra shown in Fig. 3.11 (the identified Raman modes are tabulated in Table 3.3), the spectral features present in the 900–600 cm^{-1} and 400–200 cm^{-1} regions are due to the Mo–O stretching and bending modes, respectively, which are evident in both thin films. However, the peaks located in regions < 200 cm^{-1} stem from lattice modes within the crystalline phases [14]. The Raman spectrum of the annealed MoO_x thin film deposited on glass has been discussed in Chapter 2.

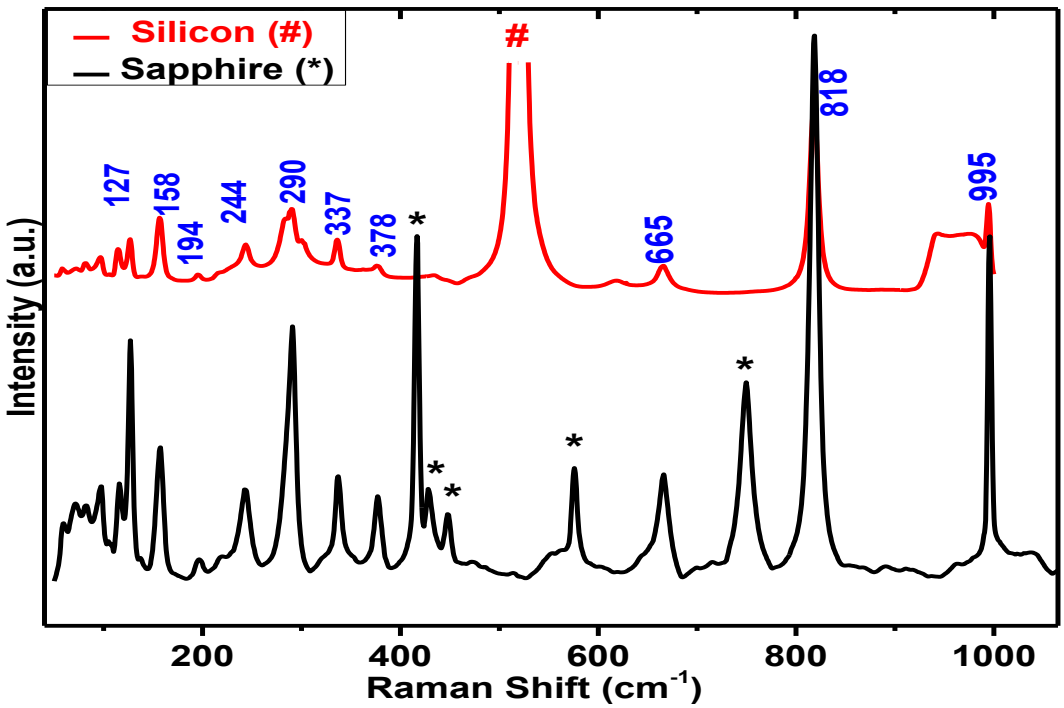

Fig. 3.11. Raman spectra (in the 50-1050 cm^{-1} range) of MoO_x thin film deposited on SiO_2/Si (Top-Red) and on the sapphire substrate (Bottom-Black), both at T_s = 300 °C, after post-annealing at 450 °C for 12 hours and 6 hours respectively. The high intensity Si single crystal Raman band (~520.7 cm^{-1}) has been cut-off for easier display of the thin film modes. The band positions of various vibrational modes in the MoO_x have been noted (blue).

Table 3.3 The Raman spectral deconvolution and analysis as compared to Literature values [35] of various oxides of molybdenum in the bulk form. The abbreviations for intensity are explained as follows: vw-very weak, w- weak, m- mild, s- sharp, vs- very sharp, sh- shoulder, br- very broad.

sapphire substrate	Si substrate (calibrated to Si peak- 520.7 cm^{-1})	Literature values [35]		
		α - MoO_3	β - MoO_3	Monoclinic MoO_2 (#), γ / η - Mo_4O_{11} (*)
72			77 (m)	
96 (m)	95 (w)	98		
115 (m),	112 (m),	115, 128	127	130(w)#
127 (s)	125 (m)			
156 (s)	154 (s)	157		163(w)*
196 (w)	194 (w)	198	194	205(s)#, 201(vw)*
219 (sh),	214 (sh)	217,	239 (vw)	229(m)#,223(vw)*/224(vw)*
243 (m)	242 (m)	246		
	282 (sh)	284 (s)	284 (vw)	269(m)*/277(m)*
290 (s)	289 (s)	290 (sh)		
337 (m)	335 (m)	337	309 (vw)	306(vw)*/322(vw)*
377 (m)	376 (w)	378	351 (w)	349(m)#, 364(s)#
			394 (vw)	
471 (br)		472		460(w)#, 452(w)*
666 (m)	665 (m)	666		
818 (vs)	817 (vs)	819		
890 (vw, br), 910 (vw, br)	962 (vw,br)		900 (w)	979(vw)*/956(w)*
995 (s)	993 (s)	995		

It is generally established that, the intense sharp peak at about 819 cm^{-1} (Fig. 3.11) is due to the doubly coordinated oxygen ($O\text{-}Mo_2$) stretching mode, which is a consequence of corner-sharing oxygens within the octahedral MoO_6 units having alternating bond lengths [14]. In addition, the peak at 666 cm^{-1} is assigned to the triply coordinated oxygen ($O\text{-}Mo_3$) stretching mode, which is due to the edge-sharing oxygens in common with three adjacently placed octahedral units. While the peak located at 995 cm^{-1} is attributed to the terminal oxygen (Mo=O) stretching mode along the a-axis and b direction within the layered orthorhombic structure of MoO_3.

As shown in Table 3.3, the band positions obtained in this work are highly consistent with the reported values. In the bending modes region, the peaks at 290 and 337 + 377 cm^{-1} are consistent with the known O-Mo-O scissoring and O=Mo=O wagging modes, respectively [32]. I have also identified Raman band features of $\alpha\text{-}Al_2O_3$ (corundum) that are present in the MoO_x/sapphire thin film. The Raman peaks located at 377, 417, 428, 447, 576, 749 cm^{-1} are most likely associated with the $2A_{1g} + 5\ E_g$ active phonon modes of the D^6_{3d} symmetry corundum space group [33, 34]. It can be noted that both the MoO_x/sapphire and the MoO_x/Si thin film (annealed for 12 hours) have very similar features apart from a redshift of ~1-3 cm^{-1}, which is most likely due to miscalibration issues.

None of the Raman bands that are consistent with known reported values of MoO_2 were identified. This may indicate a negligible MoO_2 content or it may reflect a much lower cross section of excitation of Raman modes associated with this phase [35]. The hint of other sub-stoichiometric molybdenum oxides (e.g., Mo_4O_{11}) is indicated in the broader peaked features at the [835-845 cm^{-1}, 906-911 cm^{-1}] band positions,

especially in the MoO_x/sapphire case. The low Raman scattering efficiency and the increased Rayleigh scattering below 400 cm^{-1}, of these reduced molybdenum oxides makes determination of such modes in Raman spectra difficult [35].

The relatively broad Raman features located in the frequency range that is consistent with mode associated with MoO_x sub-stoichiometric oxides may be due to increased structural disorder or relatively close and overlapping bands of these phases. Indeed, as was noted above, the total spectral information of Mo_4O_{11} is a superposition of Raman bands of corner-shared octahedral units of β–MoO_3 and the Mo^{4+} (tetravalent)-centered units present in MoO_2. Hence, the evidence for the presence of Mo_4O_{11} phase, although not entirely direct, from the Raman spectra is quite suggestive. Moreover, the feature is slightly shifted (at 72 cm^{-1}) is quite consistent with the presence of β -MoO_3 in the MoO_x/sapphire thin film, especially since this phase is an excellent Raman scatterer (see Table 3.3).

Finally, I discuss the defects in these thin films that have been detected using Raman spectroscopy. In the case of the sapphire substrate, the possibility of formation of aluminum trimolybdates ($Al_2(MoO_4)_3$) in the MoO_x thin film is evident with broad peak-like features at 1006 cm^{-1} and 380 cm^{-1} frequency values [36]. However, due to the fact that the intensity is quite low for these bands, which suggests that the content of aluminum trimolybdates may be quite low.

It has been shown that lattice oxygen defects play a major role in the selective catalysis processes [32]: The redox processes of Mo oxides are dependent on oxygen vacancies and synthesis process are designed to ensure their nominal content on the surface of these materials. The evidence of Mo^{5+} present in the MoO_x/sapphire and

MoO_x/Si thin films implies that there are oxygen vacancies located at the surface regions of the films. This, coupled with a sizable component of nanoscale morphological features inherent in the annealed thin films, makes these materials potentially suitable for selective catalytic applications.

Conclusions

My SEM and AFM results show that upon annealing at 450 °C, the MoO_x/Si thin film has a noticeably greater roughness (by 76%) than the MoO_x/sapphire thin film. In addition, the MoO_x/Si thin film had to be annealed for approximately twice the duration (~12 hours) in order to achieve a similar level of crystallinity as the MoO_x/sapphire thin film (annealed for ~ 6 hours). This may have been driven in part by the wetting characteristics of the MoO_x thin film on the two types of substrates: the wettability of molybdenum oxide on sapphire (c-axis) is greater than for Si(100). The SEM and AFM images showed the surface morphology to be considerable more uniform for the post-annealed MoO_x/sapphire thin film than for the MoO_x/Si thin film. My XRD, XPS and Raman analyses confirmed the presence of MoO_3, Mo_4O_{11}, and very likely additional sub-stoichiometric molybdenum oxide phases, although the confirmation of the latter could not be made with complete certainty. The most plausible explanation for the mixed phases is that while there was an oxygen partial pressure established in the high vacuum deposition chamber during thin film synthesis, it was at a level that enabled deposition of stoichiometric and sub-stoichiometric molybdenum oxide phases in the thin films.

Acknowledgements

The Author would like to thank Rishi Patel of the JVIC center at MSU for making the XPS measurements and AFM imaging on all the samples. Financial support has been provided partially by Graduate College at MSU.

References

[1]M. Anpo, T.S.T. Suzuki, Y. Kubokawa, F. Tanaka, S. Yamashita, Photoluminescence Evidence for the Influence of Symmetry of Molybdenum Ions upon Photocatalytic Activity, J. Phys. Chem. 88 (1984) 5778-5779.

[2]S. Hariharan, K. Saravanan, P. Balaya, α-MoO_3: A high performance anode material for sodium-ion batteries, Electrochem. Communications 31 (2013) 5–9.

[3]C.S. Hsu, C.C. Chan, H.T. Huang, C.H. Peng, W.C. Hsu, Electrochromic properties of nanocrystalline MoO_3 thin films, Thin Solid Films 516 (2008) 4839–4844.

[4]C.G. Granqvist, Handbook of Inorganic Electrochromic Materials, first ed., Elsevier, Amsterdam 1995.

[5]T. He, J. Yao, Photochromism of molybdenum oxide, J. Photochem. and Photobiol. C: Photochem. Rev. 4 (2003) 125-143.

[6]S.S. Sunu, E. Prabhu, V. Jayaraman, K.I. Gnanasekar, T. Gnanasekaran, Gas sensing properties of PLD made MoO_3 films, Sens. And Actuators B 94 (2003) 189–196.

[7]W.S. Kim, H.C. Kim, S.H. Hong, Gas sensing properties of MoO_3 nanoparticles synthesized by solvothermal method, J. Nanopart. Res. 12 (2010) 1889–1896.

[8]H. Yan, P. Song, S. Zhang, Z. Yang, Q. Wang, Facile fabrication and enhanced gas sensing properties of hierarchical MoO_3 nanostructures, RSC Advances 5 (2015) 72728-72735.

[9]T.A. Patterson, J.C. Carver, D.E. Leyden, D.M. Hercules, A Surface Study of Cobalt-Molybdena-Alumina Catalysts Using X-Ray Photoelectron Spectroscopy, J. Phys. Chem. 80 (1976) 1700-1708.

[10]N.S. McIntyre, D.D. Johnston, L.L. Coatsworth, R.D. Davidson, X-ray Photoelectron Spectroscopic Studies of Thin Film Oxides of Cobalt and Molybdenum, Surf. And Interface Analysis 15 (1990) 265-272.

[11]E. M. McCarron (III), β-MoO_3: a Metastable Analogue of WO_3, J. Chem. Soc., Chem. Commun. 4 (1986) 336-338.

[12]D.D. Yao, J.Z. Ou, K. Latham, S. Zhuiykov, A.P. O'Mullane, K. Kalantar-Zadeh, Electrodeposited α- and β-Phase MoO_3 Films and Investigation of Their Gasochromic Properties, Cryst. Growth Des. 12 (2012) 1865-1870.

[13]M. Onoda, H. Fujishita, Y. Matsuda, M. Sato, Charge density waves Mo_nO_{3n-1}, Synthetic Metals 19 (1987) 947-952.

[14]G.A. Nazri, C. Julien, Far-Infrared and Raman studies of orthorhombic MoO_3 single crystal, Solid State Ionics 53-56 (1992) 376-382.

[15]L. Kihlborg, Least squares refinement of the structure of $Mo_{17}O_{47}$, Acta. Chem. Scand. 17 (1963) 1485-1487.

[16]V. Bhosle, A. Tiwari, J. Narayan, Epitaxial growth and properties of MoO_x ($2<x<2.75$) films, J. Appl. Phys. 97 (2005) 083539.

[17]V. Eyert, R. Horny, K.H. Hock, S. Horn, Embedded Peierls instability and the electronic structure of MoO_2, J. Phys.: Condens. Matt. 12 (2000) 4923-4946.

[18]X. Liu, J. Yang, W. Hou, J. Wang, Y. Nuli, Highly Reversible Lithium-ions Storage of Molybdenum Dioxide Nanoplates for High Power Lithium-ion Batteries, Chem. Sus. Chem. 8 (2015) 2621–2624.

[19]M.A.C. Lopez, L.A. Alarcon, Structural transformations in MoO_x thin films grown by pulsed laser deposition, Appl. Phys. A 78 (2004) 59–65.

[20]J. Baltrusaitis, B.M. Sanchez, V. Fernandez, R. Veenstra, N. Dukstiene, A. Roberts, N. Fairley, Generalized molybdenum oxide surface chemical state XPS determination via informed amorphous sample model, Appl. Surface Science 326 (2015) 151-161.

[21]C.V. Ramana, C.M. Julien, Chemical and electrochemical properties of molybdenum oxide thin films prepared by reactive pulsed-laser assisted deposition, Chem. Phys. Lett. 428 (2006) 114–118.

[22]N. Illyaskutty, S. Sreedhar, G.S. Kumar, H. Kohler, M. Schwotzer, C. Natzeck, V.P.M. Pillai, Alteration of architecture of MoO_3 nanostructures on arbitrary substrates: growth kinetics, spectroscopic and gas sensing properties, Nanoscale 6 (2014) 13882–13894.

[23]T.S. Sian, G.B. Reddy, Optical, structural and photoelectron spectroscopic studies on amorphous and crystalline molybdenum oxide thin films, Sol. Energy Mater. and Sol. Cells 82 (2004) 375-386.

[24]J.A. Redenius, Femtosecond Laser-Induced Oxide Formation on Molybdenum Thin Films in Varying Low-Pressure Oxygen Environments, UNIVERSITY OF CALIFORNIA, July 2015.

[25]C.V. Ramana, V.V. Atuchin, V.G. Kesler, V.A. Kochubey, L.D. Pokrovsky, V. Shutthanandan, U. Becker, R.C. Ewing, Growth and surface characterization of sputter-deposited molybdenum oxide thin films, Appl. Surface Science 253 (2007) 5368-5374.

[26]G.G. Allogho, P.V. Ashrit, Wettability and photochromic behavior of Molybdenum oxide thin films, Thin Solid Films 520 (2012) 2326–2330.

[27]E. Comini, G. Faglia, G. Sberveglieri, C. Cantalini, M. Passacantando, S. Santucci, Y. Li, W. Wlodarski, W. Qu, Carbon monoxide response of molybdenum oxide thin films deposited by different techniques, Sens. And Actuators B 68 (2000) 168-174.

[28]F. Werfel, E. Minni, Photoemission study of the electronic structure of Mo and Mo oxides, J. Phys. C: Solid State Phys. 16 (1983) 6091-6100.

[29]N.A. Chernova, M. Roppolo, A.C. Dillonb, M.S. Whittingham, Layered vanadium and molybdenum oxides: batteries and electrochromics, J. Mater. Chem. 19 (2009) 2526–2552.

[30]N.A. Dhas, A. Gedanken, Characterization of Sonochemically Prepared Unsupported and Silica-Supported Nanostructured Pentavalent Molybdenum Oxide, J. Phys. Chem. B 101 (1997) 9495-9503.

[31]J.W. He, X. Xu, J.S. Corneille, D.W. Goodman, X-ray photoelectron spectroscopic characterization of ultra-thin silicon oxide films on a Mo(100) surface, Surf. Science 279 (1992) 119-126.

[32]G. Mestl, P. Ruiz, B. Delmon, H. Knozinger, Oxygen-Exchange Properties of MoO_3: An in Situ Raman Spectroscopy Study, J. Phys. Chem. (1994) 11269-11275.

[33]M. Kadleikova, J. Breza, M. Vesely, Raman spectra of synthetic sapphire, Microelectron. J. 32 (2001) 955-958.

[34]S.P.S. Porto, R.S. Krishnan, Raman Effect of Corundum, J. Chem. Phys. 47 (1967) 1009-1012.

[35]K.A. Olson, Laser photodeposition of molybdenum oxide thin films from organometallic precursors, IOWA STATE- Chemical Engineering Commons, 1989.

[36]D.S. Zingg, L.E. Makovsky, R.E. Tischer, F.R. Brown, S. David, M. Hercules, A Surface Spectroscopic Study of Molybdenum-Alumina Catalysts Using X-ray Photoelectron, Ion-Scattering, and Raman Spectroscopies, J. Phys. Chem. 84 (1980) 2898-2906.

Supplementary Information (SI)

Surface Profilometry. Thickness measurements were performed using a Veeco Dektak 150 instrument. The stylus radius used was 12.5 μm with a horizontal scan range of up to 2 mm. The scan resolution was kept to a minimum of 0.033 μm while the stylus tip force of 3 mg was employed. All the measurements were recorded after performing a

vertical calibration using a 10 µm (100 kÅ) calibration standard in the 6.5 µm measurement range. Thickness data was analyzed and interpreted using both Dektak 150 software and Origin pro 8.5.1. The Average Step Height function (ASH) in the Dektak 150 software gave the thickness of the non-uniform thin films after leveling the data using known substrate positions markers.

SEM-EDX of As-Deposited Thin Films. The MoO_x thin film on sapphire substrate was very smooth with holes and dislodged particles at few positions, as shown in Fig. S3.1 (a), at a magnification of 35,676 X. The morphology is not developed in the as-deposited film even for T_s = 300 °C. Although EDX analysis for elemental quantification is not reliable enough for exact stoichiometric determination, a higher working distance spectrum acquired (Fig. S3.1 (b)) shows the presence of film constituents O, Mo along with Al counted from the substrate, in the ratios of ~66.31, 10.52 and 23.16 at% respectively.

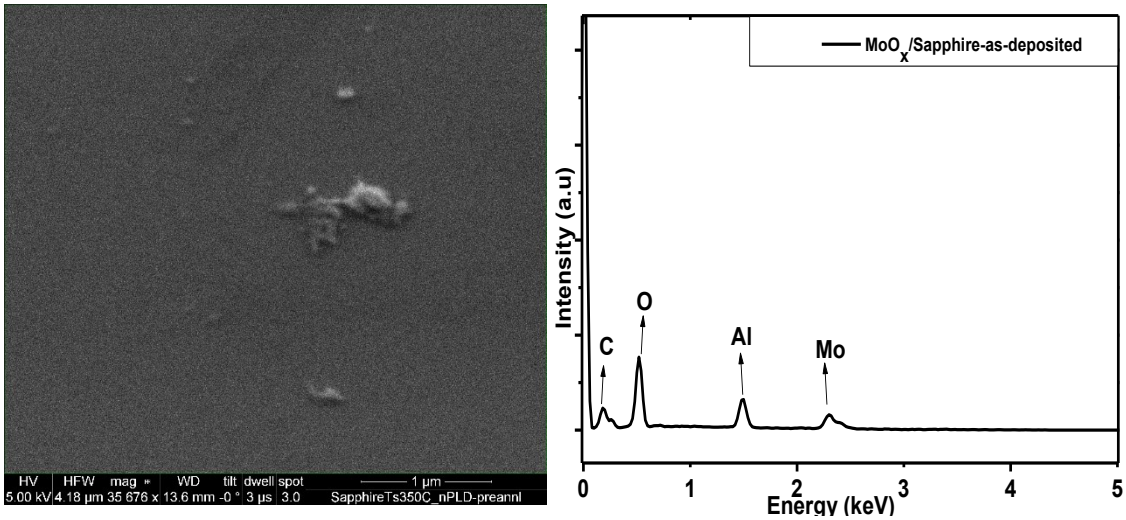

Figure S3.1. The morphology of the MoO_x/sapphire thin films in the as-deposited condition (a), which shows only smooth surface and the elemental quantification using SEM-EDX (b) at higher working distance (W.D=13.6 mm) and 5 keV.

XRD Data of As-Deposited Thin Films. The MoO_x thin films on both the substrates showed unique features, although being highly amorphous. While the $MoO_x/SiO_2/Si$ film show only a high intensity peak of the Si single crystalline plane reflection, it does show a defined amorphous nature (Fig. S3.2(a)). Conversely, the MoO_x film on sapphire substrate exhibits a mixed amorphous and crystalline nature. The high intensity corundum structure reflections can be seen here (Fig. S3.2(b)).

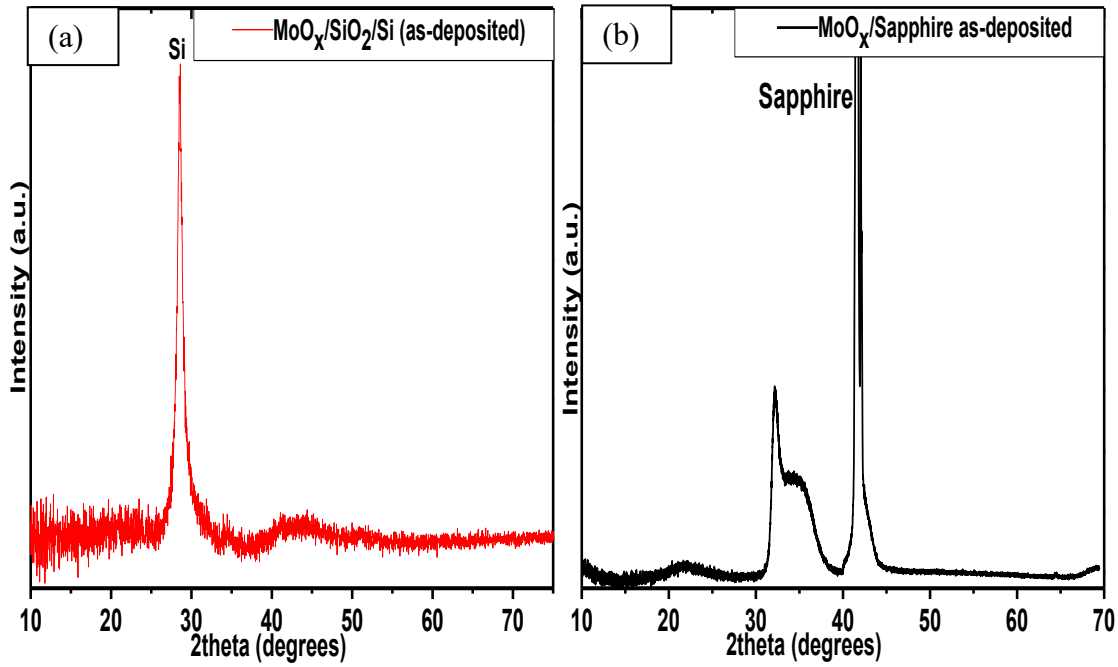

Figure S3.2. (a) A typical XRD pattern of $MoO_x/SiO_2/Si$ film in the as-deposited condition shows only the peak of Si substrate other than the majorly amorphous background. (b) The XRD pattern with unique features of mixed-amorphous/crystalline features in the thin film deposited on sapphire substrate.

Additional XPS Analysis Results. The XPS fitting analysis results of $MoO_x/SiO_2/Si$ are presented in Table S3.1. Both the HR spectrum of O1s and Mo3d were fitted subsequently following the same procedure as mentioned for the thin film on sapphire substrate in the Results section. Additionally, Table S3.2 shows the results of the

XPS survey scan fitting analysis of the $MoO_x/SiO_2/Si$ thin film. The results indicate a higher amount of Si species (SiO_2 and Si) also being detected, which may point to the presence of larger gaps in the thin films as visualized in the SEM images as well, which is indeed a direct result of the lower wettability of the thin film.

Table S3.1. Summary of fitting results of the high-resolution XPS spectra measured from $MoO_x/SiO_2/Si$ thin film. All the peak components were fitted with a Line shape based on Gaussian-Lorentzian product formula, GL(30) where the percentage of Lorentzian peak shape is indicated in the parenthesis. The standard deviation of peak areas calculated from 400 individual spectra was generated by Monte Carlo simulation-assisted peak analyses utilized within the CasaXPS software.

HR Spectrum type	Component peak	Position	FWHM	Area	%Area	%Area St. Dev.
Mo 3d	Mo^{6+} $3d_{5/2}$	231.80	2.000	149.73	39.10	0.081
	Mo^{6+} $3d_{3/2}$	234.93	1.785	99.87	26.08	0.054
	Mo^{x+} $3d_{5/2}$	230.94	1.024	80.00	20.89	0.015
	Mo^{x+} $3d_{5/2}$	234.07	1.047	53.36	13.93	0.010
O 1s	Mo^{6+} - O	530.98	2.061	286.77	17.85	0.353
	Mo^{x+} - O	529.19	1.391	115.43	7.19	0.137
	Si - O (SiO_2)	532.63	1.799	1203.95	74.96	0.302

However, the thickness of the oxide layer (SiO_2) is limited to only a few monolayers, a considerable amount of O1s (at%) is associated to this oxide layer. The results shown here (Table S3.2) are achieved from considering only the oxide component out of the Si2p region, assuming they are clearly separated and no counts are lost to the background creation. All other parameter considerations have been consistent with the fitting of sapphire substrate based thin film.

Table S3.2. Summary of the XPS survey scan elemental quantification measured from molybdenum oxide thin film on silicon substrate. The atomic concentration data (at% conc.) along with the Standard Deviation (% St. Dev) has been obtained by using a Shirley background.

Name	Position	FWHM	Area	at% Conc.	% St.Dev.[1]
O 1s	532.76	2.26	1589.15	69.74	1.09
Mo 3d	231.26	2.37	425.84	5.76	1.12
Si 2p (SiO_2 only)	103.76	1.82	155.62	24.49	0.32

[1] Standard deviation of the % Atomic concentrations of each of the elements.

Macroscopic Images of Thin Films before and After Annealing. Good resolution photographs of the thin films on the substrates have been recorded to show the color change before and after annealing cycles. Attached here are the images of the Si substrate (Fig. S3.3) and sapphire substrate (Fig. S3.4).

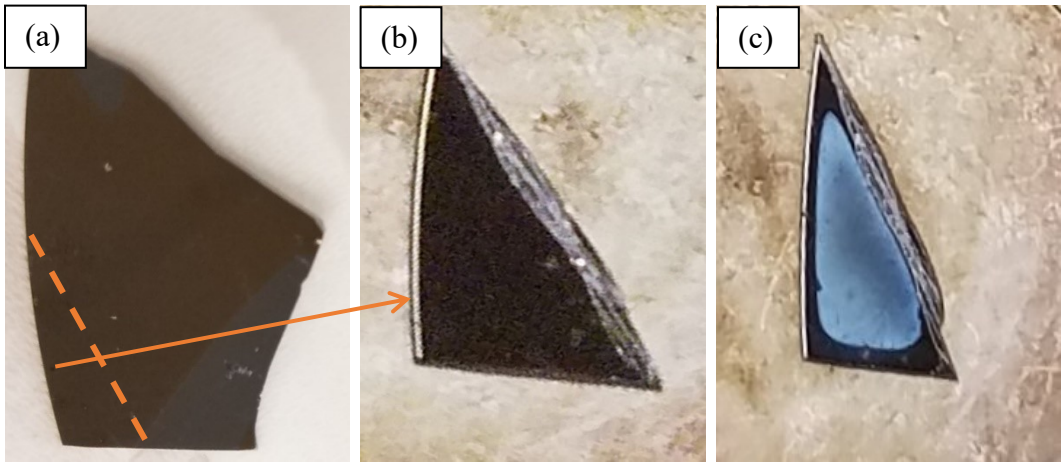

Figure S3.3. Photographs of the MoO_x thin film on Si (100) substrate in the, (a) as-deposited condition (fresh from the PLD chamber, which was used for annealing after cutting on one edge (as shown), in (b) just before annealing on the Linkam Stage, and finally upon annealing at 450 °C, for 12 hours.

It is evident that the Si-based film has a peculiar blue color development upon annealing at 450 °C for both annealing times of 6 and 12 hours. There is a definitive effect of thermocoloration occurring in this thin film. However, further optical band gap studies would quantify the effect and potentially show whether there was any possible formation of water stabilized (H) pentavalent Mo_2O_5.

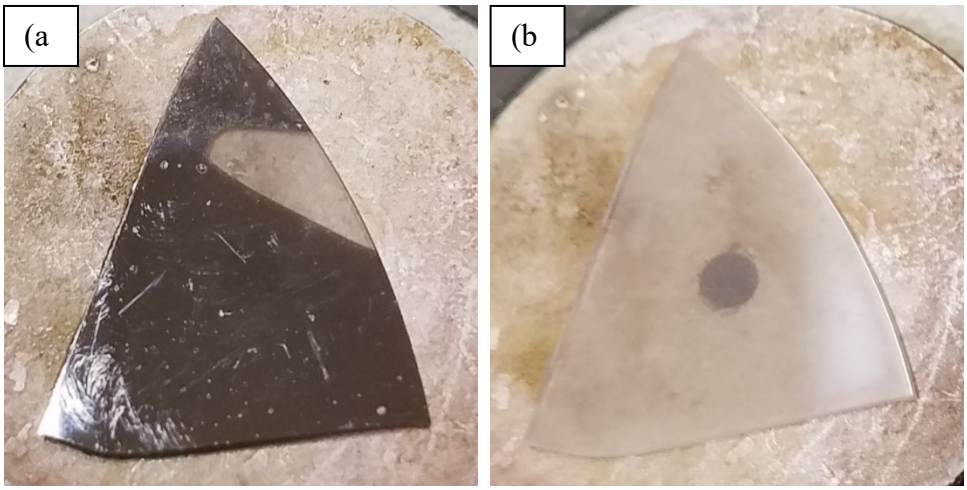

Figure S3.4. The MoO_x/sapphire thin film in the (a) as–deposited condition just before annealing, and (b) just after annealing at 450 °C for 6 hours.

Conversely, in the sapphire based thin film, there was only bleaching of the initial dark color state, probably pointing toward formation of nearly stoichiometric thin film ($MoO_{2.9}$). This film is highly transparent and most likely the reflectivity in the post-annealed can be associated to the polished side of the sapphire substrate. Again, this conjecture can be proven based on the study of the optical parameters in comparison with the literature values.

CHAPTER 4: SUMMARY

To conclude, in Chapter 2, this work describes a characterization study of molybdenum oxide thin films produced using two essentially different pulsed laser deposition (PLD) techniques, differing substantially in the pulse duration and energy deposited per unit time on the targets. Hence, the ablation mechanisms are unique to the laser being used, either in the femtosecond or nanosecond pulse regime. The femtosecond pulse based-PLD technique produced favorable thin films for any surface-related applications, based on the fact that higher surface area to volume ratio was attained for molybdenum oxide thin film deposited on glass. SEM results provide evidence for improved nano-structured texture with higher roughness on the MoO_x thin films deposited on glass by use of the femtosecond PLD than on the MoO_x/glass thin film deposited using the nanosecond PLD technique. As part of a preliminary research finding, it was observed that both thin films (f-PLD and n-PLD) comprised of an admixture of hexavalent (MoO_3) and tetravalent (MoO_2) stable phases of molybdenum oxide. XRD, Raman and XPS analyses confirm the presence of both the orthorhombic and distorted rutile-type crystal structures, consistent with the MoO_3 and MoO_2 phases, respectively.

In Chapter 3, an additional characterization study of the influence of substrate epitaxy and processing conditions showed that the interface affect the morphological development of MoO_x ($2<x<3$) thin films during the growth as well as subsequent thermal treatment processes. Upon annealing at 450 °C, the MoO_x/sapphire thin film, which has an ideal stoichiometry closer to that of MoO_3 (O: Mo ~ 2.90 vs 2.84 for the

MoO_x/Si thin film, as shown from XPS analysis), had less roughness and 3D growth whereas the MoO_x/Si thin film was more dominated by the 3D growth aspect as shown using SEM and AFM analyses (R_q ~ 23.2 nm for the MoO_x/Si and R_q ~ 13 nm for the MoO_x/sapphire thin film). The XRD analysis revealed presence of the orthorhombic α-MoO_3 and mixed phases of Mo_4O_{11} along with most likely additional MoO_x phases, in the post-annealed MoO_x/Si and MoO_x/sapphire thin films. Raman spectroscopy has corroborated the presence of the Mo_4O_{11} phase, which contain a combination of hexavalent and tetravalent Mo species. My Raman results are consistent with the content of the MoO_x sub-stoichiometric phases being greater in the MoO_x/sapphire thin film.

REFERENCES FOR INTRODUCTION

[1]M.S.B. Darby, Femtosecond Pulsed Laser Deposition, University of Southampton, 2009.

[2]S. Eliezer, N. Eliaz, E. Grossman, D. Fisher, I. Gouzman, Z. Henis, S. Pecker, Y. Horovitz, M. Fraenkel, Synthesis of nanoparticles with femtosecond laser pulses, Phys. Rev. B 69 (2004) 144119 (1-6).

[3]D.B. Chrisey, G.K. Hubler, Pulsed Laser Deposition of Thin Films, John Wiley & Sons, New York, 1994.

[4]P. Waters, The Effects Of Moisture On Thin Film Delamination And Adhesion, University of South Florida, 2005.

[5]Intechopen, http://www.intechopen.com/books/plasma-science-and-technology-progress-in-physical-states-and-chemical-reactions/laser-induced-plasma-and-its-applications, 2016

[6]R. Eason, Ultrafast Laser Ablation and Film Deposition, in: D.B. Chrisey, G.K. Hubler, Pulsed Laser Deposition of Thin Films, John Wiley & Sons, New Jersey, 2007, pp. 99-127.

[7]T. He, J. Yao, Photochromism of molybdenum oxide, J. Photochem. and Photobiol. C: Photochem. Rev. 4 (2003) 125-143.

[8]A. Hojabri, F. Hajakbari, A.E. Meibodi, Structural and optical properties of nanocrystalline orthorhombic MoO_3 thin films prepared at different annealing temperatures, J. Theor. Appl. Phys. 9 (2015) 67-73.

[9]G.A. Nazri, C. Julien, Far-Infrared and Raman studies of orthorhombic MoO_3 single crystal, Solid State Ionics 53-56 (1992) 376-382.

[10]J. Zhou, N. Lin, L. Wang, K. Zhang, Y. Zhu, Y. Qian, Synthesis of hexagonal MoO_3 nanorods and a study of their electrochemical performance as anode materials for lithium-ion batteries, J. Mat. Chem. A 3 (2015) 7463-7468.

[11]J.A. Redenius, Femtosecond Laser-Induced Oxide Formation on Molybdenum Thin Films in Varying Low-Pressure Oxygen Environments, UNIVERSITY OF CALIFORNIA, July 2015.

[12]M.F.A. Kuhaili, S.M.A. Durrani, I.A. Bakhtiari, A.M.A. Shukri, Optical constants and thermocoloration of pulsed laser deposited molybdenum oxide thin films, Opt. Commun. 283 (2010) 2857-2862.

[13]A. Pardo, J. Torres, Substrate and annealing temperature effects on the crystallographic and optical properties of MoO_3 thin films prepared by laser assisted evaporation." Thin Solid Films 520 (2012) 1709-1717.

[14]A. Soultati, M. Vasilopoulou, G. Papadimitropoulos, A. Douvas, I. Kostis, I. Karystinos, S. Kennou, G. Skoulatakis, D. Davazoglou, Impact of microwave post deposition annealing on the crystallization of amorphous hydrogenated perovskites. The case of the three-dimensional tungsten and of the two-dimensional molybdenum oxide films, Thin Solid Films 615 (2016) 329-337.

[15]H.K. Puppala, A.T. Pelton, R.A. Mayanovic. "A Comparative Characterization Study of Molybdenum Oxide Thin Films Grown Using Femtosecond and Nanosecond Pulsed Laser Deposition." MRS Advances 1 (2016): 2585-2590.